

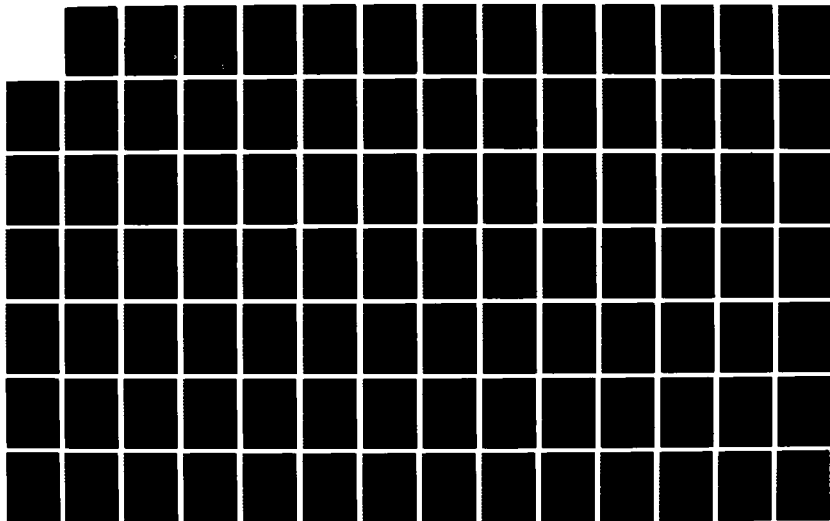
AD-A189 559

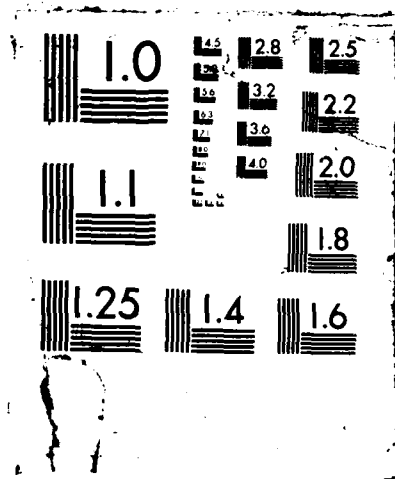
OPTIMAL SELECTION OF GLOBAL POSITIONING SYSTEM SET TO  
MINIMIZE EMITTER LO. (U) AIR FORCE INST OF TECH  
WRIGHT-PATTERSON AFB OH SCHOOL OF ENGI.. S G PETERS  
DEC 87 AFIT/ENG/GE/87D-51 F/G 17/7

1/2

UNCLASSIFIED

NL





DTIC FILE COPY

1

AD-A189 559



OPTIMAL SELECTION OF GLOBAL  
POSITIONING SYSTEM SET TO MINIMIZE  
EMITTER LOCATION ERRORS

Stephen G. Peters  
Captain, USAF

AFIT/ENG/GE/87D-51

DTIC  
ELECTE  
MAR 03 1988

DEPARTMENT OF THE AIR FORCE  
AIR UNIVERSITY

**AIR FORCE INSTITUTE OF TECHNOLOGY**

Wright-Patterson Air Force Base, Ohio

**DISTRIBUTION STATEMENT A**

Approved for public release;  
Distribution Unlimited

88 3 01 143

①  
AFIT/GE/ENG/87D-51

OPTIMAL SELECTION OF GLOBAL  
POSITIONING SYSTEM SET TO MINIMIZE  
EMITTER LOCATION ERRORS

Stephen G. Peters  
Captain, USAF

AFIT/ENG/GE/87D-51

DISTRIBUTION STATEMENT A

Approved for public release;  
Distribution Unlimited

DTIC  
ELECTE  
MAR 03 1988  
S H D

AFIT/GE/ENG/87D-51

OPTIMAL SELECTION OF GLOBAL POSITIONING SYSTEM SET  
TO MINIMIZE EMITTER LOCATION ERRORS

THESIS

Presented to the Faculty of the School of Engineering  
of the Air Force Institute of Technology  
Air University  
In Partial Fulfillment of the  
Requirements for the Degree of  
Master of Science in Electrical Engineering

Stephen G. Peters, B.S.  
Captain, USAF

December 1987

Approved for public release; distribution unlimited

## Preface

I would like to thank my thesis advisor, Lt Col Zdzislaw Lewantowicz, for the guidance he gave me and the faith he had in me during this research effort. I would also especially like to thank Dr. Peter Maybeck and Col Daniel Biezdad for timely inputs to keep me on the right track.

A special thanks is due to Capt Rodney Bain, who provided support when it was most needed. He is not only a good friend, but a true brother in Christ as well.

Most of all, I would like to thank my wife, Wendy, for the loving support and assistance she gave me during those months when the end seemed so far away. She handled the stress and put up with me through the worst times; without her this thesis would have been impossible to accomplish.

Stephen G. Peters



Accession For	
NTIS GRA&I	<input checked="checked" type="checkbox"/>
DTIC TAB	<input type="checkbox"/>
Unannounced	<input type="checkbox"/>
Justification	
By	
Distribution	
Availability	
Dist	
A-1	

## Table of Contents

	Page
Preface . . . . .	ii
List of Figures . . . . .	v
List of Tables . . . . .	vi
Abstract . . . . .	vii
I. Introduction . . . . .	1
Background . . . . .	1
Problem and Scope . . . . .	2
Summary of Current Knowledge . . . . .	3
Assumptions . . . . .	4
General Approach . . . . .	5
Overview . . . . .	8
II. Error Dynamics and Measurement Model . . . . .	10
Introduction . . . . .	10
Observer Navigation System . . . . .	12
The Emitter Measurement System . . . . .	16
Observer Navigation and Emitter Measurement . . . . .	17
III. Estimator and Cost Function Development . . . . .	35
Introduction . . . . .	35
Estimator Development . . . . .	36
Cost Function Formulation . . . . .	39
Cost Gradient Formulation . . . . .	42
Minimum Cost Search Technique . . . . .	46
IV. Results . . . . .	53
Introduction . . . . .	53
Four Satellite Optimization . . . . .	54
Three Satellite Optimization . . . . .	65
Two Satellite Optimization . . . . .	74
Satellite Selection Algorithm . . . . .	79
V. Conclusions and Recommendations . . . . .	82
Conclusions . . . . .	82
Recommendations . . . . .	83

	Page
Bibliography . . . . .	85
Appendix A: Cost Gradient Function Derivation . . . . .	A.1
Vita . . . . .	V.1

## List of Figures

Figure	Page
2.1. Two Dimensional Navigation Measurement Geometry . .	23
2.2. Two Dimensional Emitter Measurement Geometry . . .	32
3.1. Geometry for LOS Elevation Constraint . . . . .	45
3.2. Steepest Descent Search Technique . . . . .	49
3.3. Projection of Gradient onto Tangent . . . . .	51
4.1. Four Satellite Initial Configuration . . . . .	55
4.2. CEP Behavior During Filter Iterations . . . . .	58
4.3. CEP Behavior at First Local Minimum . . . . .	59
4.4. CEP Transient Behavior . . . . .	60
4.5. Four Satellite Final Configuration . . . . .	62
4.6. Four Satellite Trajectory . . . . .	64
4.7. Pseudo Three Satellite Final Geometry . . . . .	67
4.8. Pseudo Three Satellite Trajectory . . . . .	69
4.9. Three Satellite Final Geometry . . . . .	71
4.10. Three Satellite Trajectory . . . . .	73
4.11. Two Satellite Final Geometry . . . . .	76
4.12. Two Satellite Trajectory . . . . .	78

### List of Tables

Table	Page
4.1 Four Satellite Initial Positions . . . . .	56
4.2 Four Satellite Initial Error Ellipse Parameters .	56
4.3 Four Satellite Final Positions . . . . .	63
4.4 Four Satellite Final Error Ellipse Parameters . .	63
4.5 Pseudo Three Satellite Final Positions . . . . .	68
4.6 Pseudo Three Satellite Error Ellipse Parameters .	68
4.7 Three Satellite Final Positions . . . . .	72
4.8 Three Satellite Error Ellipse Parameters . . . . .	72
4.9 Two Satellite Final Positions . . . . .	77
4.10 Two Satellite Error Ellipse Parameters . . . . .	77

Abstract

The use of the Global Positioning System (GPS) as a navigation aid for aircraft attempting to locate a ground-based electromagnetic energy emitter is studied. In particular, the satellite geometry which yields minimum errors in the emitter location estimation for four different satellite availability cases is explored. This geometry, in general, is not the same as that which yields minimum aircraft navigation errors. Satellite selection criteria are identified and serve as a basis for selection algorithm development.

The research shows that emitter location errors can be significantly reduced by selecting satellites based on the criteria presented in this study. Three satellite performance is found to be nearly as good as that obtained using four satellites and, for the two satellite case, emitter location is still better for some period of time than that obtained using four satellites selected to minimize Geometric Dilution of Precision (GDOP).

# OPTIMAL SELECTION OF GLOBAL POSITIONING SYSTEM SET TO MINIMIZE EMITTER LOCATION ERRORS

## I. INTRODUCTION

### 1.1 BACKGROUND

The use of aircraft equipped with electro-magnetic energy receivers to determine the location of an emitter has many military, as well as civilian, applications. Missions such as strategic and tactical reconnaissance, as well as airborne search and rescue, require accurate determination of an emitter location. The difficulty faced by these airborne collectors is that in order to determine an emitter location precisely, they must establish their own position very accurately. This difficulty is compounded by the fact that, for many applications, a global positioning capability is required. Although many navigation systems such as LORAN and OMEGA provide substantial capability, the Global Positioning System (GPS) provides continuous global coverage with much greater accuracy. However, in order to obtain highly accurate observer position information, it is necessary that the airborne platform select the appropriate satellites from the available constellation of satellites which will yield optimum emitter location solution geometry. Ideally, the satellite selection criterion should optimize the accuracy of the emitter location estimation.

## 1.2 PROBLEM AND SCOPE

The problem is to determine the positions of three airborne collectors and four GPS satellites such that errors in the estimate of emitter location will be minimized. In this case, optimum position is defined as that position which results in a minimum value for the emitter location estimate mean squared miss distance (MSMD), or alternatively, the circular error probable (CEP). The MSMD is a scalar cost function of the emitter location errors, which in turn is a function of the satellite position geometry expressed in the Kalman filter measurement equation. The local minimum CEP cost value is obtained using a steepest descent gradient search algorithm.

This study examines the impact of both satellite positions and collector positions on emitter location errors. It also investigates emitter location accuracy after degrading to three and two satellite operation. Additionally, an algorithm is developed which selects the optimum satellite configuration for minimum emitter location errors. Note that the goal is not to develop the "best possible" emitter location system, but to determine the optimal satellite geometry which minimizes emitter location error. Therefore, a highly elaborate truth model is not required.

### 1.3 SUMMARY OF CURRENT KNOWLEDGE

The NAVSTAR Global Positioning System is a space-based radio-positioning navigation system which provides highly accurate three-dimensional position and velocity information on a global basis to a very large number of users (9:146). In general, at least four satellites are required to solve the four time-difference-of-arrival equations for the three dimensional position and the user receiver clock error (1:85). Since the GPS generally allows the user to view six or more satellites at any given time, it is necessary to select the combination of satellites that will give the most accurate position information (3:8). The effect that satellite geometry has on ranging accuracy can be expressed in terms of Geometric Dilution of Precision (GDOP) (3:8). An algorithm which maximizes navigation accuracy selects the combination of four satellites that yields the smallest value of GDOP (3:8). It should be noted that although the minimum GDOP criteria results in minimum user position errors, it "... does not generally result in minimum emitter location errors" (4:64). This is due to two factors. One is that vertical collector position errors contribute negligibly to emitter location errors since the emitter is assumed to be on the surface of the earth. The second is that the collector position errors are mapped through the nonlinear hyperbolic functions to the emitter location errors (10). The use of joint estimation of emitter position with observer

position produces emitter location errors which are significantly smaller than estimates based on satellite selection using minimum GDOP criteria (4:93). It is also noted that the joint estimator significantly outperforms the two stage estimation process where the observer navigation problem is solved first, followed by solution for the emitter position. The price which is paid for the gains obtained by using a joint estimator is an increase in computational loading. During his research at the Massachusetts Institute of Technology, Lewantowicz (4) investigated system performance when using only three satellites and found that emitter location accuracy was very nearly the same as that obtained using four satellites. Additionally, he demonstrated that degraded operation using only two satellites and a precise clock yields an acceptably accurate emitter location solution.

A number of assumptions necessary to define and adequately limit the problem are presented in the next section.

#### 1.4 ASSUMPTIONS

The following assumptions are made at the outset of the problem:

1. There are three airborne collectors operating simultaneously.
2. Each collector platform has a high grade Inertial Navigation System (INS) with barometric altimeter data available. The

external altitude measurement is available to stabilize the inherently unstable vertical channel of the INS.

3. Each collector has measurements available from four GPS satellites. Further, each observer uses the same four satellites for updates. This is a reasonable assumption since the three platforms are operating in the same geographic area and will "see" essentially the same constellation of available satellites.

4. The GPS satellites selected should lie at or above five degrees elevation from the local horizon measured from the center of the collector geometry. Lower elevation angles increase ranging errors due to propagation effects.

5. The collectors use a passive emitter locating method known as the hyperbolic location system (10).

6. A constrained emitter-collector geometry is assumed. This assumption narrows the problem to that where the approximate emitter location in general is initially known or crudely measured.

#### 1.5 GENERAL APPROACH

Parameter optimization is used to solve a set of emitter location problems assuming various satellite availability constraints as outlined by the following.

### OPTIMUM SATELLITE POSITION

During this portion of the study the four GPS satellite positions are selected from among an infinite set on the orbital sphere using the cost gradient search. The collectors executed their predetermined orbits. The cost is formulated as a function of GPS satellite positions and is computed using the Kalman filter covariance matrix function. The filter covariance matrix is a function of the measurement observation matrix, which in turn depends on the satellite positions. Thus, for a steady-state Kalman filter solution, the cost function depends only on the satellite positions. Therefore, the gradient vector of this scalar cost function indicates the magnitude and "direction of movement" for each satellite at update time. The navigation Kalman filter is allowed to reach steady state from the same initial conditions at each cost computation point before satellite "movements" are computed. It is hypothesized that information retained by iterating the filter only one time between satellite movements without reinitializing the Kalman filter may have produced overly-optimistic CEPs as obtained by Lewantowicz in his research (4). His motivation for iterating only one time is the computational savings in the minimum cost search.

### THREE SATELLITE PERFORMANCE

Of the four satellites, three are moved to optimum positions for this portion of the study, while the fourth

satellite remains fixed overhead to simulate the availability of a precise clock onboard each collector platform. A second analysis is accomplished using information from only three satellites to determine the validity of the hypothesis that the overhead satellite can be used to simulate a precise clock in a three satellite problem. A comparison is made between the results obtained using these two approaches.

#### TWO SATELLITE PERFORMANCE

This portion of the study is very similar to the three satellite case. Given Kalman filter estimates of user clock bias and user clock drift obtained using measurements from four satellites, the number of visible satellites is reduced to only two and the satellite positions are again optimized. Comparisons are made with previous simulations to determine the feasibility of two satellite operation.

#### DEVELOPMENT OF A SELECTION ALGORITHM

The results of the optimum satellite position analysis are then used to construct a selection algorithm. The behavior of the scalar cost as a function of satellite geometries are studied to determine the characteristics of an "optimum satellite geometry" and selection criteria are established.

## 1.6 THESIS OVERVIEW

The following chapters describe the problem structure, the mechanics used in solving the problem, and the results obtained.

Chapter 2 develops the error dynamics and measurement models used by the emitter locating system. The observer navigation error state vector is augmented with the error states associated with the emitter measurement process to obtain the system error state vector. Measurement models are formulated for observer navigation measurements, as well as emitter measurements, and are linearized for use in linear estimation.

Chapter 3 builds the structure of the discrete-time extended Kalman filter which is used as the estimator for this study. The cost function, based upon emitter location mean squared miss distance, is developed as a function of the GPS satellite positions. The emitter location CEP is also computed. Finally, the minimum cost search technique used in this study, the steepest descent weighted gradient algorithm, is described.

Chapter 4 presents the results obtained when the GPS satellites are moved to optimum positions, minimizing the error in the emitter location estimate. The three satellite performance is shown to be essentially the same as that obtained using four satellites. Further, the use of only two satellites

and filter estimates for user clock parameters yields reasonable emitter location performance. Satellite selection criteria are established based on the results obtained in the four satellite optimization cases.

Chapter 5 presents conclusions and recommendations arising from this study.

## II. ERROR DYNAMICS AND MEASUREMENT MODELS

### 2.1 INTRODUCTION

In general, locating an electromagnetic emitter requires a method for determining the observer's position, as well as a method for distinguishing signals intercepted from an emitter. For the simplified case of a stationary observer, the observer position can be very accurately determined by means of a precise survey. However, for such applications as airborne search and rescue operations, the observers must move in order to provide the required coverage of the vast areas involved. The problem of determining the position of these moving observers requires a navigation system capable of providing highly accurate position information on a global basis.

In this study, the system used by each observer to provide this high quality position data is a high grade inertial navigation system (INS) which is updated by measurements from four GPS space vehicles (SV) and stabilized by measurements from a barometric altimeter. As pointed out in Section 1.4, the GPS satellites selected lie at or above five degrees elevation from the local horizon and each observer uses the same four satellites for updates. Note that the following models and derivations correspond to those used and developed by Lewantowicz in his thesis (4).

The method used to analyze the performance of the emitter location system is a linearized error covariance analysis of the estimated errors. To perform this analysis, the state vector representing the actual system state is given by  $\underline{x}_a(t)$  and the estimate of the state vector at the same time  $t$  is given by  $\hat{\underline{x}}(t)$ . The error state vector,  $\underline{x}(t)$ , can then be defined as

$$\underline{x}(t) = \underline{x}_a(t) - \hat{\underline{x}}(t) \quad (2-1)$$

which satisfies in general the vector differential equation

$$\begin{aligned} \dot{\underline{x}}(t) &= \underline{f}(\underline{x}, t) + G \underline{w}(t) \\ \underline{x}(0) &= \underline{x}_0 \end{aligned} \quad (2-2)$$

where  $\underline{f}$  is a time-varying vector valued function of  $\underline{x}(t)$  describing the error state dynamics. The matrix  $G$  is the time invariant noise distribution matrix, and  $\underline{w}$  is an independent zero-mean white Gaussian noise process with covariance kernel

$$E[\underline{w}(t)\underline{w}^T(t + \tau)] = Q(t) \delta(\tau) \quad (2-3)$$

where  $E$  is the expectation operator,  $Q$  is a diagonal matrix, and  $\delta$  is the Dirac delta function.

The measurement process for the estimator is well modelled by

$$\underline{z}(t) = \underline{h}(\underline{x}, t) + \underline{v}(t) \quad (2-4)$$

where  $\underline{h}$  is a time-varying vector valued function of the error state  $\underline{x}$ . The measurement noise  $\underline{v}(t)$  is an independent zero-mean white Gaussian noise process with covariance kernel

$$E[\underline{v}(t)\underline{v}^T(t + \tau)] = R \delta(\tau) \quad (2-5)$$

where  $R$  is a diagonal matrix.

Given this system model, an extended Kalman filter is used to estimate navigation errors. This filter is discussed in Section 3.2. System dynamics and measurement models for navigation and emitter location are discussed in Sections 2.2 through 2.4.

## 2.2 OBSERVER NAVIGATION SYSTEM

A number of systems are available which can provide navigation data to airborne observers. These include time-difference-of-arrival (TDOA) type systems such as LORAN and OMEGA and range measurement type systems using Distance Measuring Equipment (DME) measurements to surveyed stations on the ground. These systems are, in general, limited by combinations of accuracy, availability or areas of coverage. A performance improvement over these systems is provided by GPS.

The NAVSTAR GPS, when fully operational, will consist of a constellation of 18 SVs, 3 in each of 6 orbital planes (9:146). The GPS has potential for providing highly accurate three-dimensional position and velocity information along with Coordinated Universal Time (UTC) to a very large number of suitably equipped users. The orientation of the satellite orbits generally allows the observer to view six or more satellites at any given time, thus providing adequate navigation information on a global basis (3:18). The GPS SV transmits an encoded navigation message from which the receiver can determine the pseudo-range to the SV with a very high degree of accuracy. The locus of points for each pseudo-range measurement describes a sphere whose center is at the SV. The point where three spheres intersect provides the observer with position information in three dimensions. Since the observer generally uses a fairly inaccurate crystal clock, a fourth pseudo-range measurement is used to determine the user clock bias. Most of the error sources associated with the GPS can be effectively minimized by error modelling and the use of Kalman filtering to estimate these errors. As a result, the GPS is capable of providing much more accurate position information than most other navigation systems. Because of this high degree of accuracy and the global positioning capability of the GPS, a high-grade INS is combined with the GPS to form the navigator which is used for the emitter locating system in this study.

### 2.2.1 THE INERTIAL NAVIGATION SYSTEM

The INS system errors are modelled using 16 states, forming the state vectors  $\underline{x}_1$ ,  $\underline{x}_2$ , and  $\underline{x}_3$ . Note that there are three INS error state vectors since each of the three airborne observers has its own INS. Each of these state vectors is defined as follows (4):

$$\underline{x}_1 = \begin{bmatrix} \text{East position error} \\ \text{North position error} \\ \text{Vertical position error} \\ \text{East velocity error} \\ \text{North velocity error} \\ \text{Vertical velocity error} \\ \text{Roll error (east axis)} \\ \text{Roll error (north axis)} \\ \text{Roll error (vertical axis)} \\ \text{Barometric altimeter error} \\ \text{Barometric sea level pressure variation} \\ \text{East accelerometer bias} \\ \text{North accelerometer bias} \\ \text{East gyro bias} \\ \text{North gyro bias} \\ \text{Vertical gyro bias} \end{bmatrix} \quad (2-6)$$

State vectors  $\underline{x}_2$  and  $\underline{x}_3$  are defined in the same manner. It should be noted that the roll, pitch and yaw data in each body frame are transformed to the East-North-Vertical (ENV) navigation frame for each observer (4:17).

### 2.2.2 THE GLOBAL POSITIONING SYSTEM

The measurements available to update the inertial navigation system are pseudo-range measurements to the GPS SV represented by

$$R_{ij} = c t_{ij} \quad (2-7)$$

where  $R_{ij}$  is the pseudo-range from the  $i$ -th observer to the  $j$ -th SV,  $c$  is the speed of light, and  $t_{ij}$  is the travel time of the signal. Because there are errors inherent in the system, this pseudo-range measurement does not only represent the actual line of sight (LOS) range to the SV, but includes several errors. The error sources modelled for this study are uncalibrated propagation errors in each GPS receiver channel, uncalibrated offset and drift errors in each observer clock, code loop interchannel biases, and LOS errors. These errors form the state vectors  $x_4$  through  $x_8$  described by

$x_4$	12 states for receiver propagation errors
$x_5$	3 states for clock offsets
$x_6$	3 states for clock drifts
$x_7$	12 states for code loop interchannel bias
$x_8$	4 states for LOS biases (1 per SV)

The augmented error state vector is formed by combining all the error states as

$$x^T = [x_1^T, x_2^T, x_3^T, x_4^T, x_5^T, x_6^T, x_7^T, x_8^T] \quad (2-8)$$

The resulting error state column vector is of dimension 82.

Although models of higher dimensionality exist, the model described is adequate for this study. Such assumptions as straight, level, unaccelerated flight at high altitude reduce the effect of other error sources allowing lower state vector dimensionality.

### 2.3 THE EMITTER MEASUREMENT SYSTEM

States which describe the errors associated with the emitter measurement process are added to the model. These states are the emitter position, emitter-signal receiver time delay calibration error for each observer, and the error in modelling tropospheric delay along the line of sight from each observer to the emitter. These errors form the state vectors  $x_9$  through  $x_{11}$  and are described as

$x_9$	3 states for emitter position errors
$x_{10}$	3 states for receiver calibration errors
$x_{11}$	3 states for tropospheric delay errors

The total augmented error state vector,  $x(t)$  is formed by augmenting state vectors  $x_9$  through  $x_{11}$  to Eqn. (2-8)

$$x^T = [x_1^T, x_2^T, x_3^T, x_4^T, x_5^T, x_6^T, x_7^T, x_8^T, x_9^T, x_{10}^T, x_{11}^T] \quad (2-9)$$

This final error state vector is of dimension 91.

Note that this formulation of the error state vector allows joint estimation of emitter position with observer position so that all available information is processed jointly at each computation step. The result of this is that the solution is optimal in the minimum mean-squared error (MMSE) sense (6). Each measurement updates both the navigation position and the emitter location. As a result, the emitter measurement can be used to reduce navigation errors. The consequence of choosing

the joint estimation scheme over a two-stage estimator (4) is an increase in required computations. For this study, the increased performance of the joint estimator justified the increased computational burden.

With the models for the error state dynamics and noise inputs now developed, the next step is to model the measurements for the navigation update and the emitter update.

## 2.4 OBSERVER NAVIGATION AND EMITTER MEASUREMENTS

### 2.4.1 OBSERVER NAVIGATION MEASUREMENTS

The actual navigation measurement is the pseudo-range from the observer to the GPS SV defined as the transit time of the signal scaled by the speed of light. Each GPS signal carries an encoded navigation message containing SV ephemeris data which allows the position of the SV to be determined very accurately. With this information, the observer can solve four equations in four unknowns. These unknowns are the three position components of the navigation error state vector and the user clock bias error.

In addition to the inherent system errors in the GPS, other error sources affect the accuracy of the pseudo-range measurement. The significant errors are modelled and discussed

in this section. The errors induced by atmospheric delay result primarily from ionospheric refraction. The change in apparent path length brought about by ionospheric refraction can be substantially reduced by employing dual frequency compensation since each SV transmits two frequencies,  $f_1$  and  $f_2$ . The two frequency compensation is based on the fact that the ionospheric delay  $\delta\tau$  is frequency dependent

$$\delta\tau = \frac{K}{f^2} \quad (2-10)$$

where

$K$  = environmental constant  
 $f$  = carrier frequency

Let  $\tilde{\Delta t}_1$  denote transit time measurement at frequency  $f_1$  and write it as (4:23)

$$\tilde{\Delta t}_1 = \Delta t + \delta\tau_1 + r_1 \quad (2-11)$$

where

$\Delta t$  = the transit time of the signal (uncorrupted)  
 $\delta\tau_1$  = ionospheric delay at frequency  $f_1$   
 $r_1$  = time measurement error due to other sources

Forming the ratio

$$\frac{\delta\tau_2}{\delta\tau_1} = \frac{k/f_2^2}{k/f_1^2} = \left[ \frac{f_2^2}{f_1^2} \right]^{-1} \quad (2-12)$$

yields

$$\delta\tau_2 = \frac{f_1^2}{f_2^2} \delta\tau_1 \quad (2-13)$$

Rewriting Eqn. (2-11) for frequency  $f_2$

$$\tilde{\Delta}t_2 = \Delta t + \delta\tau_2 + r_2 \quad (2-14)$$

Next, define the measurement difference between frequency  $f_1$  and  $f_2$ ,  $\delta\tilde{\Delta}t$  as

$$\delta\tilde{\Delta}t = \tilde{\Delta}t_1 - \tilde{\Delta}t_2 \quad (2-15)$$

Solving for  $\delta\tilde{\Delta}t$  by substituting Eqn. (2-11) and (2-14) into (2-15) yields

$$\begin{aligned} \delta\tilde{\Delta}t &= \Delta t + \delta\tau_1 + r_1 - \Delta t - \delta\tau_2 - r_2 \\ &= \delta\tau_1 - \delta\tau_2 + r_1 - r_2 \end{aligned} \quad (2-16)$$

Substituting (2-13) for  $\delta\tau_2$  produces

$$\begin{aligned} \delta\tilde{\Delta}t &= \delta\tau_1 - \frac{f_1^2}{f_2^2} \delta\tau_1 + r_1 - r_2 \\ &= (1 - \alpha^2) \delta\tau_1 + r_1 - r_2 \end{aligned} \quad (2-17)$$

where

$$\alpha = \frac{f_1}{f_2}$$

Writing the compensated time delay measurement at frequency  $f_1$

$$\tilde{\Delta t}^c = \tilde{\Delta t}_1 - \frac{\delta \tilde{\Delta t}}{1 - \alpha^2} \quad (2-18)$$

Substituting (2-17) and (2-11) into (2-18) gives

$$\begin{aligned} \tilde{\Delta t}^c &= \Delta t + \delta \tau_1 + r_1 - \frac{\delta \tilde{\Delta t}}{1 - \alpha^2} \\ &= \Delta t + \delta \tau_1 + r_1 - \delta \tau_1 - \frac{r_1 - r_2}{1 - \alpha^2} \\ &= \Delta t + \frac{r_1 (1 - \alpha^2) - r_1 + r_2}{1 - \alpha^2} \\ &= \Delta t - \frac{\alpha^2}{1 - \alpha^2} r_1 + \frac{1}{1 - \alpha^2} r_2 \end{aligned} \quad (2-19)$$

Note that the ionospheric delay dependence has vanished, but  $r_1$  and  $r_2$  are still undefined.

Let

$$r_1 = \gamma_1 + \Delta t_{1c} + v_1 \quad (2-20)$$

$$r_2 = \gamma_2 + \Delta t_{2c} + v_2 \quad (2-21)$$

where  $\gamma_1$  and  $\gamma_2$  are the GPS code loop measurement bias errors in the two receivers. These errors are modelled as elements of state vector  $\underline{x}_4$  while  $\Delta t_c$ , the user clock bias error, is modelled by  $\underline{x}_5$ , as described in Section 2.2.2. The terms  $v_1$  and  $v_2$  represent zero mean, white Gaussian measurement noise.

Substituting Eqn (2-20) and (2-21) into (2-19) to obtain

$$\tilde{\Delta t}^c = \Delta t + \delta t_c - \frac{\alpha^2}{1 - \alpha^2} (\gamma_1 + v_1) + \frac{1}{(1 - \alpha^2)} (\gamma_2 + v_2) \quad (2-22)$$

where

$$\delta t_c = (\Delta t_{2c} - \alpha^2 \Delta t_{1c}) / (1 - \alpha^2)$$

Since the compensated time delay measurement has been determined, the ionospheric error compensated pseudo-range measurement is obtained simply by multiplying by the speed of light,  $c$

$$c\tilde{\Delta t}^c = c\Delta t + c\delta t_c - \frac{c\alpha^2}{1 - \alpha^2} (\gamma_1 + v_1) + \frac{c}{(1 - \alpha^2)} (\gamma_2 + v_2)$$

or

$$\tilde{R}^C = R + \delta R_C - \frac{c\alpha^2}{1 - \alpha^2} (\gamma_1 + v_1) + \frac{c}{(1 - \alpha^2)} (\gamma_2 + v_2) \quad (2-23)$$

With this range measurement model, the next step generates the observation model for the range measurement between the  $i$ -th observer and the  $j$ -th GPS SV.

Let  $P_S(j)$  denote the position vector of the  $j$ -th GPS SV expressed in the earth-centered earth-fixed (ECEF) coordinate frame. The line-of-sight (LOS) vector from the  $i$ -th observer to the  $j$ -th SV is then the vector  $P_{AS}(i,j)$ . This geometry is shown for the two-dimensional case in Figure 2.1. From this figure it is seen that

$$P_{AS}(i,j) = P_S(j) - P_A(i) \quad (2-24)$$

The range  $R(i,j)$  is a nonlinear function of  $P_{AS}(i,j)$ . If the computed LOS vector is defined as  $P_{AS}$ , then the range is given by

$$\begin{aligned} R(i,j) &= |P_{AS}(i,j)| \\ &= |P_S(j) - P_A(i)| \\ &= [P_{AS}^T(i,j) P_{AS}(i,j)]^{1/2} \end{aligned} \quad (2-25)$$

where  $|\cdot|$  is the magnitude operator.

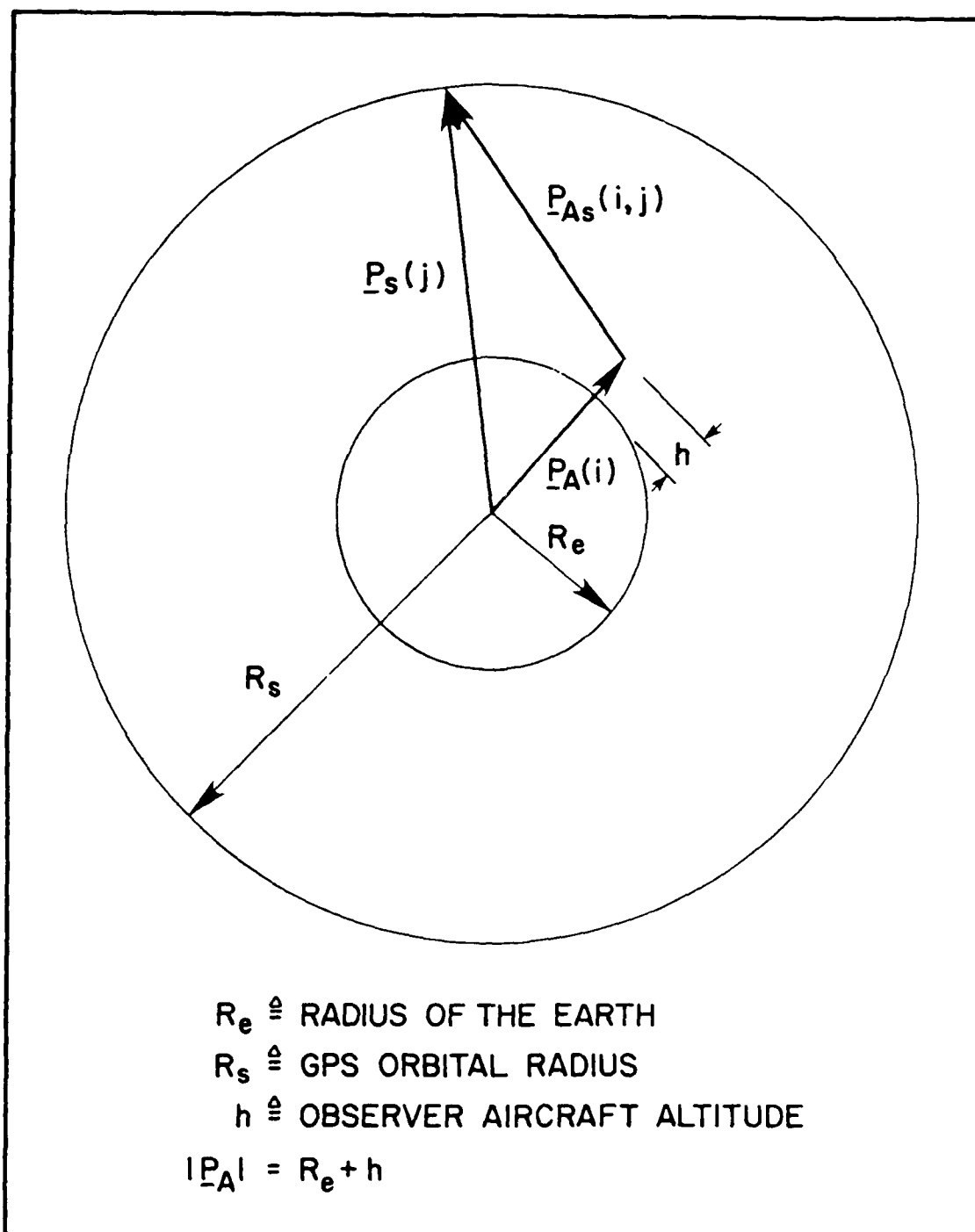


FIG. 2.1. TWO DIMENSIONAL NAVIGATION MEASUREMENT GEOMETRY

Since a linearized measurement model is required for estimation,  $\hat{R}(i,j)$  and  $R_C(i,j)$  are expanded in Taylor series about the actual positions to first order yielding (4:27)

$$\hat{R} = R + \frac{\partial R}{\partial P_S} \delta P_S + \frac{\partial R}{\partial P_A} \delta P_A \quad (2-26)$$

Taking the partial derivatives produces

$$\frac{\partial R(i,j)}{\partial P_S(j)} = \frac{P_{AS}^T(i,j)}{R(i,j)} = U_{AS}^T(i,j) \quad (2-27)$$

and

$$\frac{\partial R(i,j)}{\partial P_A(j)} = - \frac{P_{AS}^T(i,j)}{R(i,j)} = - U_{AS}^T(i,j) \quad (2-28)$$

It should be noted that the first partial derivative of the range is the unit line of sight vector. Thus, (2-26) becomes

$$\hat{R}(i,j) = R(i,j) + U_{AS}^T(i,j) [\delta P_S(j) - \delta P_A(i)] \quad (2-29)$$

The linearized measurement,  $z(i,j)$ , can be formed using (2-23) and (2-29) as

$$\begin{aligned} z(i,j) &= \tilde{R}^C(i,j) - \hat{R}(i,j) \\ &= - U_{AS}^T(i,j) [\delta P_S(j) - \delta P_A(i)] + \delta R_C(i) - \frac{c\alpha^2}{1 - \alpha^2} \cdot \\ &\quad [\gamma_1(i,j) + v_1(i,j)] + \frac{c}{1 - \alpha^2} [\gamma_2(i,j) + v_2(i,j)] \end{aligned} \quad (2-30)$$

The errors in observer position,  $\delta \underline{p}_A(i)$ , are the first three elements of the inertial navigation system error state model vectors  $\underline{x}_1$ ,  $\underline{x}_2$ , and  $\underline{x}_3$  as given by Eqn (2-6) for  $i=1, 2, 3$  respectively. The GPS position errors,  $\delta \underline{p}_S(j)$ , are modelled as unknown biases along each  $j$ -th line of sight and are represented by the error state vector  $\underline{x}_8$  described in Section 2.2.2. Thus, (2-30) can be written

$$\begin{aligned} z(i,j) = & \underline{u}_{AS}^T(i,j) \delta \underline{p}_A(i) + \delta R_C(i) - \frac{c\alpha^2}{1-\alpha^2} [\gamma_1(i,j) + v_1(i,j)] \\ & + \frac{c}{1-\alpha^2} [\gamma_2(i,j) + v_2(i,j)] + b_E(j) \end{aligned} \quad (2-31)$$

Note that the additional term  $b_E(j)$  is added to account for unmodelled LOS biases.

In order to reduce the dimension of the error state vector, the code loop errors,  $\gamma_1$  and  $\gamma_2$ , and the measurement noise terms,  $v_1$  and  $v_2$ , are combined respectively to obtain two random variables  $\gamma$  and  $v$ . By letting

$$\begin{aligned} \gamma(i,j) = & - \frac{c\alpha^2}{1-\alpha^2} \gamma_1(i,j) + \frac{c}{1-\alpha^2} \gamma_2(i,j) \\ v(i,j) = & - \frac{c\alpha^2}{1-\alpha^2} v_1(i,j) + \frac{c}{1-\alpha^2} v_2(i,j) \end{aligned}$$

Eqn (2-31) is rewritten as

$$z(i,j) = U_{AS}^T(i,j) \delta P_A(i) + \delta R_C(i) + \gamma(i,j) + v(i,j) + b(j) \quad (2-32)$$

The code loop tracking errors are modelled as first-order Markov processes such that the combined code loop dynamics are given by

$$\dot{\gamma} = -\frac{1}{\tau} \gamma + w \quad (2-33)$$

where  $\tau$  is a relatively long time constant given by

$$\tau = \frac{1}{4B_n} \quad (2-34)$$

and  $B_n$  is the noise equivalent bandwidth of the code loop tracking filter. The user clock offset error,  $\delta R_C$ , is modelled as a constant drift

$$\dot{\delta R_C} = \frac{c}{f_C} \delta f_C \quad (2-35)$$

where  $\delta f_C$  is the user clock frequency error and  $\delta f_C/f_C$  is a random constant drift bias. Thus,

$$\frac{\dot{\delta f_C}}{f_C} = 0 \quad (2-36)$$

These two states model the clock error. The equivalent pseudo-range bias term,  $b_E$ , is modelled as a random constant such that

$$\dot{b}_E = 0 \quad (2-37)$$

With the navigation measurement model now complete, the emitter measurement model is developed next.

#### 2.4.2. EMITTER MEASUREMENTS

Since the transmission time of a received emitter signal is not known a priori, the transit time cannot be used to determine the range to the emitter. The only information available to each airborne observer is the time of arrival (TOA) of the emitter signal at its receiver. For the case of the GPS SVs, the quantities of interest require that computations be done in three dimensions. However, for the case of the observers and the emitter, the planar projection of the three dimensional emitter location error ellipsoid onto the horizontal surface is the quantity of most significance. This is because it is assumed that the emitter vertical position is known with sufficient accuracy.

Using three independent measurements of the emitter signal, one from each airborne observer, three TOA's are obtained with the time differences of arrival (TDOA) defined as:

$$\tilde{TDOA}_{12} = \tilde{TOA}_1 - \tilde{TOA}_2 \quad (2-38)$$

$$\tilde{TDOA}_{23} = \tilde{TOA}_2 - \tilde{TOA}_3 \quad (2-39)$$

The measurement  $\tilde{TOA}_i$  can be written as the sum of the actual  $TOA_i$  and the measurement error  $\delta TOA_i$

$$\tilde{TOA}_i = TOA_i + \delta TOA_i \quad (2-40)$$

Substituting (2-40) into the form of (2-38)

$$\tilde{TDOA}_{ij} = TOA_i - TOA_j + \delta TOA_i - \delta TOA_j \quad (2-41)$$

Next the individual error terms making up  $\delta TOA_i$  are examined  
(4:31)

$$\delta TOA_i = \delta TROP_i + \delta REC_i + \delta CLCK_i + v_i \quad (2-42)$$

where

$\delta TROP_i$  = time delay due to errors in tropospheric model

$\delta REC_i$  = time delay due to uncalibrated receiver delay

$\delta CLCK_i$  = observer clock bias error

$v_i$  = measurement corruption noise

Next, Equation (2-42) is substituted into (2-41) yielding

$$\begin{aligned} \widetilde{TOA}_{ij} = & TOA_i - TOA_j + \delta CLCK_{ij} + \delta TROP_i - \delta TROP_j \\ & + \delta REC_i - \delta REC_j + v_{ij} \end{aligned} \quad (2-43)$$

where

$$\delta CLCK_{ij} = \delta CLCK_i - \delta CLCK_j$$

and

$$v_{ij} = v_i - v_j$$

The time difference of arrival in (2-43) is scaled by the speed of light to yield the range difference

$$\begin{aligned} \Delta \widetilde{R}(i,j) = & \Delta R(i,j) + \delta R_C(i) - \delta R_C(j) + \delta R_T(i) - \delta R_T(j) \\ & + \delta R_R(i) - \delta R_R(j) + v(i,j) \end{aligned} \quad (2-44)$$

where

$$\Delta \widetilde{R}(i,j) = c(\widetilde{TOA}_i - \widetilde{TOA}_j)$$

$$\Delta R(i,j) = c(TOA_i - TOA_j)$$

$$\delta R_C(i) = c \delta CLCK_i$$

$$\delta R_T(i) = c \delta TROP_i$$

$$\delta R_R(i) = c \delta REC_i$$

$$v(i,j) = c(v_i - v_j)$$

It should be noted that each  $v_i$  is modelled as a white Gaussian noise of mean zero and, further, that the  $v_i$ 's are independent

of each other such that

$$v_i = N [0, R]$$

and

(2-45)

$$v(i, j) = N [0, 2R]$$

where  $R$  is the variance of each  $v_i$  (4:32).

Note that the clock is assumed to be the same for the entire emitter location problem. Therefore, the same clock error states are shared for the navigation as well as the emitter solution. The error terms of  $\delta R_C$ ,  $\delta R_T$ , and  $\delta R_R$  are related to the error state vector  $\underline{x}(t)$  by noting that  $\delta R_C$  is represented by  $c\underline{x}_5$  of Section 2.2.2,  $\delta R_T$  is represented by  $c\underline{x}_{11}$  and  $\delta R_R$  is represented by  $c\underline{x}_{10}$  with  $\underline{x}_{10}$  and  $\underline{x}_{11}$  described in Section 2.3.

As with the GPS measurement development in Section 2.4.1, the next step develops the observation model from the range measurement model.

The error state observation is well modelled by

$$z(i, j) = \tilde{\Delta R}(i, j) - \hat{\Delta R}(i, j) \quad (2-46)$$

where

$\hat{\Delta R}(i, j)$  = computed or estimated measurement

Let  $\hat{\underline{P}}_E$  denote the position vector of the emitter expressed in the ECEF coordinate frame. Next, let  $\hat{\underline{P}}_A(i)$  and  $\hat{\underline{P}}_A(j)$  represent the position vectors of the i-th and j-th observer aircraft respectively, again expressed in the ECEF frame. The LOS vectors from the emitter to the i-th and j-th observer are then the vectors  $\hat{\underline{P}}_{AE}(i)$  and  $\hat{\underline{P}}_{AE}(j)$ , respectively. This measurement geometry is described in two dimensions in Fig. 2.2. It is noted from the figure that

$$\hat{\underline{P}}_{AE}(i) = \hat{\underline{P}}_E - \hat{\underline{P}}_A(i) \quad (2-47)$$

So the range difference  $\hat{\Delta R}(i,j)$  is a nonlinear function of  $\hat{\underline{P}}_{AE}(i)$  and  $\hat{\underline{P}}_{AE}(j)$ . Using these computed lines of sight vectors allows the range difference to be expressed as

$$\begin{aligned} \hat{\Delta R}(i,j) &= |\hat{\underline{P}}_{AE}(i)| - |\hat{\underline{P}}_{AE}(j)| \\ &= |\hat{\underline{P}}_E - \hat{\underline{P}}_A(i)| - |\hat{\underline{P}}_E - \hat{\underline{P}}_A(j)| \end{aligned} \quad (2-48)$$

Note that  $\hat{\underline{P}}_A(i)$  and  $\hat{\underline{P}}_A(j)$  are those estimated quantities which have been used in Equation (2-25) for deriving the navigation measurement model. Again, a linearized measurement model is required so  $\hat{\Delta R}(i,j)$  is expanded in Taylor series to first order about the actual observer and emitter positions yielding

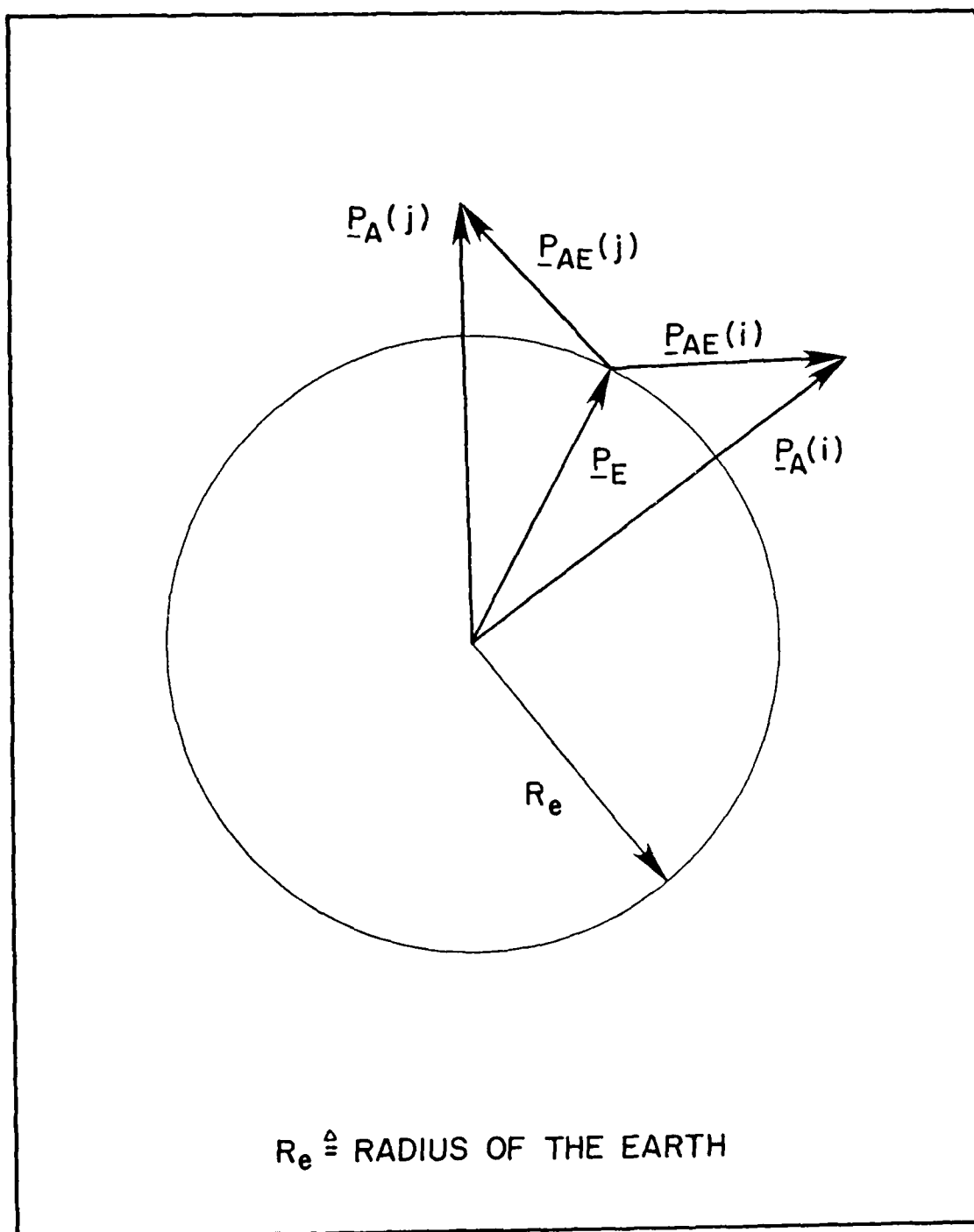


FIG. 2.2 TWO DIMENSIONAL EMITTER MEASUREMENT GEOMETRY

$$\begin{aligned}\hat{\Delta R}(i,j) = \Delta R(i,j) &+ \frac{\partial \Delta R^T(i,j)}{\partial \underline{P}_E} \delta \underline{P}_E + \frac{\partial \Delta R^T(i,j)}{\partial \underline{P}_A(i)} \delta \underline{P}_A(i) \\ &+ \frac{\partial \Delta R^T(i,j)}{\partial \underline{P}_A(j)} \delta \underline{P}_A(j)\end{aligned}\quad (2-49)$$

Evaluating each of the required partial derivatives using (2-48) yields

$$\frac{\partial \Delta R^T(i,j)}{\partial \underline{P}_E} = \frac{\partial}{\partial \underline{P}_E} [ |\underline{P}_{AE}(i)| - |\underline{P}_{AE}(j)| ] \quad (2-50)$$

Therefore, the partial derivatives of (2-49) are written as

$$\begin{aligned}\frac{\partial \Delta R^T(i,j)}{\partial \underline{P}_E} &= \frac{\underline{P}_{AE}^T(i)}{R_i} - \frac{\underline{P}_{AE}^T(j)}{R_j} \\ &= \underline{U}_{AE}^T(i) - \underline{U}_{AE}^T(j)\end{aligned}\quad (2-51)$$

Again, note that the derivatives of the magnitudes of the LOS vectors conveniently become the unit line of sight vectors; in this case from the i-th and j-th observers to the emitter.

The third term on the right hand side of (2-49) is evaluated

$$\frac{\partial \Delta R(i,j)}{\partial \underline{P}_A(i)} = - \frac{\underline{P}_{AE}^T(i)}{R_i}$$

$$= - \underline{U}_{AE}^T(i) \quad (2-52)$$

Finally, the last term in (2-49) is

$$\begin{aligned} \frac{\partial \Delta R(i,j)}{\partial \underline{P}_A(j)} &= \frac{\underline{P}_{AE}^T(j)}{R_i} \\ &= \underline{U}_{AE}^T(j) \end{aligned} \quad (2-53)$$

Substituting (2-44) and (2-49), with the partial derivatives evaluated, into (2-46) produces the required error measurement equation

$$\begin{aligned} z(i,j) &= \delta R_C(i) - \delta R_C(j) + \delta R_T(i) - \delta R_T(j) \\ &+ \delta R_R(i) - \delta R_R(j) + v(i,j) \\ &- [\underline{U}_{AE}^T(i) - \underline{U}_{AE}^T(j)] \delta \underline{P}_E + \underline{U}_{AE}^T(i) \delta \underline{P}_A(i) \\ &- \underline{U}_{AE}^T(j) \delta \underline{P}_A(j) \end{aligned} \quad (2-54)$$

This completes the model development for system error dynamics, including the INS, GPS and emitter location system errors, as well as the measurement models for navigation and emitter measurements. In the next chapter the estimator, cost function, and cost gradient are developed.

### III. ESTIMATOR AND COST FUNCTION DEVELOPMENT

#### 3.1 INTRODUCTION

The models developed in Chapter 2 are the cornerstones upon which an estimator can be built. The purpose of this estimator is to provide a time history of the statistical properties of the error state vector  $\underline{x}(t)$  as it is propagated forward in time from some initial condition  $\underline{x}(t_0) = \underline{x}_0$ . For this study, a discrete-time, time-varying estimator is used. Because the measurement model is nonlinear, an extended Kalman filter was selected and is described in Section 3.2 of this chapter.

In order to develop a cost function for an emitter locating system, it is necessary to examine the figures of merit available for evaluating the performance of such a system. The most obvious, and most crucial, performance criterion is the accuracy with which the system can estimate the actual emitter location. Although the accuracy of this estimate can be expressed in any of several ways, the mean squared miss distance serves as the basis for cost function development in this study. The development of the cost function and some of its limitations are described in Section 3.3. Using the derived cost function, the cost gradient is developed in Section 3.4. Finally, the minimum cost search technique used in this study is presented in Section 3.5.

### 3.2 ESTIMATOR DEVELOPMENT

In order to use the Kalman filter as the estimator for this study, certain assumptions need to be made. These assumptions are that (1) the state dynamics model and the measurement model are linear, (2) system dynamic driving noise and measurement corruption noise processes are well described by Gaussian processes, and (3) all system noise processes are well modelled as "white". With these assumptions, the extended Kalman filter is developed (6).

First, the nonlinear error state dynamics model given by (2-2) is expanded in Taylor series about the current best estimate of the error state vector and truncated to first order terms

$$\underline{f}(\underline{x}, t) = \underline{f}[\hat{\underline{x}}(t), t] + \left. \frac{\partial \underline{f}(\underline{x}, t)}{\partial \underline{x}} \right|_{\underline{x} = \hat{\underline{x}}(t)} \delta \underline{x} \quad (3-1)$$

where  $\delta \underline{x}$  represents the error state vector. Defining

$$F(t) = \left. \frac{\partial \underline{f}(\underline{x}, t)}{\partial \underline{x}} \right|_{\underline{x} = \hat{\underline{x}}(t)} \quad (3-2)$$

produces the linearized dynamics model

$$\dot{\underline{x}} = F(t) \underline{x} + G \underline{w} \quad (3-3)$$

Note that for the first time interval, the nominal point for expansion is  $\hat{\underline{x}}(t_0) = \hat{\underline{x}}_0$ . Also note that the model is relinearized about the new estimate each time it is computed. This allows the nominal trajectory to be updated on a continuing basis to ensure that deviations from the nominal remain small.

Using the same approach for  $\underline{h}(\underline{x}, t)$ , the nonlinear measurement vector given by (2-4) is linearized. Define

$$H(t) = \left. \frac{\partial \underline{h}(\underline{x}, t)}{\partial \underline{x}} \right|_{\underline{x} = \hat{\underline{x}}(t)} \quad (3-4)$$

resulting in the linearized measurement equation

$$\underline{z}(t_i) = H(t_i) \underline{x} + \underline{v} \quad (3-5)$$

Forming the equivalent discrete-time system model, Eqn (3-3) becomes the stochastic difference equation

$$\underline{x}(t_{i+1}) = \Phi(t_{i+1}, t_i) \underline{x}(t_i) + \underline{w}_d(t_i) \quad (3-6)$$

where

$$\begin{aligned} E [\underline{w}_d(t_i)] &= \underline{0} \\ E [\underline{w}_d(t_i) \underline{w}_d(t_i)] &= Q_d(t_{i+1}, t_i) \end{aligned} \quad (3-7)$$

and

$$Q_d(t, t_i) = \int_{t_i}^t \Phi(t, r) G(r) Q(r) G^T(r) \Phi^T(t, r) dr \quad (3-8)$$

Note that  $\Phi(t, t_i)$  is the state transition matrix such that

$$\Phi(t_0, t_0) = I \quad (3-9)$$

$$\Phi(t_2, t_0) = \Phi(t_2, t_1) \Phi(t_1, t_0) \quad (3-10)$$

The measurement equation (3-5) already models discrete-time measurements, so it remains unchanged.

Having satisfied the three initial assumptions in this section, the Kalman filter equations are stated.

The estimate is propagated forward in time using (6):

$$\begin{aligned} \hat{x}(t_{i+1}^-) &= \hat{x}(t_i^+) + \int_{t_i}^{t_{i+1}} f[\hat{x}(t/t_i), t] dt \\ P(t_{i+1}^-) &= \Phi(t_{i+1}, t_i) P(t_i^+) \Phi^T(t_{i+1}, t_i) + Q_d(t_i) \end{aligned} \quad (3-11)$$

where

$$P(t_i^+ = 0) = P_0 \quad (3-12)$$

and the measurement update equations are given by (6):

$$K(t_i) = P(t_i^-) H^T(t_i) [H(t_i) P(t_i^-) H^T(t_i) + R(t_i)]^{-1} \quad (3-13)$$

$$\hat{x}(t_i^+) = \hat{x}(t_i^-) + K(t_i) [z_i - H(t_i) \hat{x}(t_i^-)] \quad (3-14)$$

$$P(t_i^+) = P(t_i^-) - K(t_i) H(t_i) P(t_i^-) \quad (3-15)$$

Using the assumptions presented at the beginning of this section allows the conditional probability density function,  $f_{x/z}(\xi, Z)$ , to be completely described by only the first two moments. This provides mathematical tractability and allows a time history of  $\underline{x}(t)$  to be generated, conditioned on all measurements up through time  $t$ , by propagating only the conditional mean and the covariance. The second moment, the error covariance matrix  $\underline{P}(t)$ , is used for the error covariance analysis in this study.

### 3.3 COST FUNCTION FORMULATION

In general, the figure of merit used to evaluate the performance of an emitter locating system is the accuracy with which the system can estimate the actual emitter location in three dimensions. For this study, the problem reduces to an essentially two-dimensional, or planar problem, due to the assumption that the vertical emitter position is known precisely. Therefore, the quantity of real interest is the emitter location error ellipse formed by the projection of the error ellipsoid onto the  $x$ - $y$  plane. The error ellipse used in this study is the circular error probable (CEP) contour, which is a contour of equal joint probability density that yields a probability of 0.5 when integration of the probability density function is carried out over the area enclosed by the contour.

The expression used for the CEP in this study is (4:40)

$$\text{CEP} = 0.5887 (\sigma_x + \sigma_y) \quad (3-16)$$

Note that this expression represents the CEP for an actual circle where  $\sigma_x$  and  $\sigma_y$ , the semi-major and semi-minor axes, are equal. For the more realistic case where the equal probability density contour is an ellipse with  $\sigma_x \neq \sigma_y$ , it is found that (3-16) approximates the true CEP to within three percent as long as

$$0.15 < \frac{\sigma_x}{\sigma_y} < 1.0 \quad (3-17)$$

Because of the validity of the approximation given by Eqn (3-16), the cost function may be defined in terms of CEP. Since the CEP is a function of  $\sigma_x$  and  $\sigma_y$ , the error covariance matrix,  $\underline{P}(t)$ , is examined to see how these quantities can be obtained. First, the two states of interest are the emitter location errors in the horizontal plane,  $x(83)$  and  $x(84)$ . The four elements of  $\underline{P}(t)$  needed to obtain  $\sigma_x$  and  $\sigma_y$  are given by

$$\underline{P}_{\text{emit}} = \begin{vmatrix} P_t(83,83) & P_t(83,84) \\ P_t(84,83) & P_t(84,84) \end{vmatrix} \quad (3-18)$$

or in simplified notation

$$P_{\text{emit}} = \begin{vmatrix} P_{11} & P_{12} \\ P_{21} & P_{22} \end{vmatrix} \quad (3-19)$$

Note that the eigenvalues of  $P_{\text{emit}}$  are the magnitudes of the principal axes of the error ellipse and the eigenvectors represent the principal axes directions. If it is assumed that the principal axes are rotated only a very small amount from the coordinate axes, then the cross covariance terms  $P_{12}$  and  $P_{21}$  are approximately zero and the diagonal terms are given as

$$P_{11} = \sigma_x \quad \text{and} \quad P_{22} = \sigma_y \quad (3-20)$$

Now it is possible to define a mean squared miss distance cost function,  $J$ , as

$$\begin{aligned} J(P_S) &= \sigma_x + \sigma_y \\ &= P_{11} + P_{22} \end{aligned} \quad (3-21)$$

which is related to the root mean square (RMS) miss distance by

$$\text{RMS} = J^{1/2} \quad (3-22)$$

An alternate method is to define the cost function in terms of the CEP such that  $J_{\text{CEP}}$  is given by

$$J_{\text{CEP}}(\underline{P}_S) = \sigma_x + \sigma_y \quad (3-23)$$

which is directly related to CEP by

$$\text{CEP} = 0.5887 J_{\text{CEP}}(\underline{P}_S) \quad (3-24)$$

As pointed out by Lewantowicz (4), the cost gradient for mean squared miss distance computation  $g(\underline{P}_S)$ , is easier than the computation for the CEP cost gradient,  $g_{\text{CEP}}(\underline{P}_S)$ . For this reason,  $J(\underline{P}_S)$  given by (3-21), the mean squared miss distance cost, is the cost function which is actually minimized in this study. The results are presented in terms of both CEP and RMS miss distance.

Note that the error covariance matrix,  $\underline{P}(t_1^+)$ , is iterated from the initial conditions to steady-state values at each step of the cost search. This prevents the accumulation of past SV position related information in the cross-covariance terms of the P matrix as the satellite geometry changes.

Using the cost function described by (3-21), the cost gradient is developed.

### 3.4 COST GRADIENT FORMULATION

To accomplish the MSMD cost gradient computation it is convenient to express (3-21) in compact matrix notation where

$$\begin{aligned}
J(\underline{P}_s) &= \text{tr} [ E \ P_t ] \\
&= P_t(83,83) + P_t(84,84)
\end{aligned}
\tag{3-25}$$

where

E is a square 91 x 91 matrix of all zeros, except for 1's in the 83rd and 84th diagonal positions.

and

$P_t$  is the error covariance matrix at time t

From (3-25) and (3-11), it can be seen that the cost J is a function of the vector  $\underline{P}_s$  described in Section 2.4.1. This  $\underline{P}_s$  starts out as a 12 dimensional vector describing the three-dimensional position of each of 4 satellites in the ECEF frame. Note that the vector  $\underline{P}_s$  is constrained by the fixed orbital radius of the GPS satellites. For the j-th satellite, the vector is constrained such that (4:68)

$$x_j = (R_s^2 - y_j^2 - z_j^2)^{1/2} \tag{3-26}$$

The geometry chosen is such that the x-axis of the ECEF frame passes through the "center" of the observer geometry, where the center is defined as a point equidistant from the endpoints of a line segment connecting observer 1 and observer 3. The y-z plane forms the two-dimensional space onto which the SV and observer positions are projected. Note that for projection purposes, the center of the observer geometry is located along

the x-axis at an altitude  $h$  above the surface of the earth. Incorporating the effect of this constraint yields an eight dimensional parameter vector  $\underline{P}_S$ .

$$\underline{P}_S = [ Y_1, z_1, Y_2, z_2, Y_3, z_3, Y_4, z_4 ] \quad (3-27)$$

For each SV, this two-dimensional space is further constrained by the initial assumption that satellites used must lie at or above five degrees elevation from the local horizon measured from the intersection of the y-z axes. The result of this constraint maps all allowable satellite positions into a circle of radius  $R_C$  centered at the origin of the y-z coordinate system.

Fig. 3.1 depicts a triangle with angles A, B, and C with sides opposite these angles given by a, b, and c respectively. From this figure it can be seen that

$$| R_C | = R_S \cos \beta \quad (3-28)$$

Referring to Fig. 3.1, find the angle C using the law of sines

$$\frac{R_S}{\sin B} = \frac{R_e+h}{\sin C} \quad (3-29)$$

where  $B = 95^\circ$ .

solving for the angle C yields:

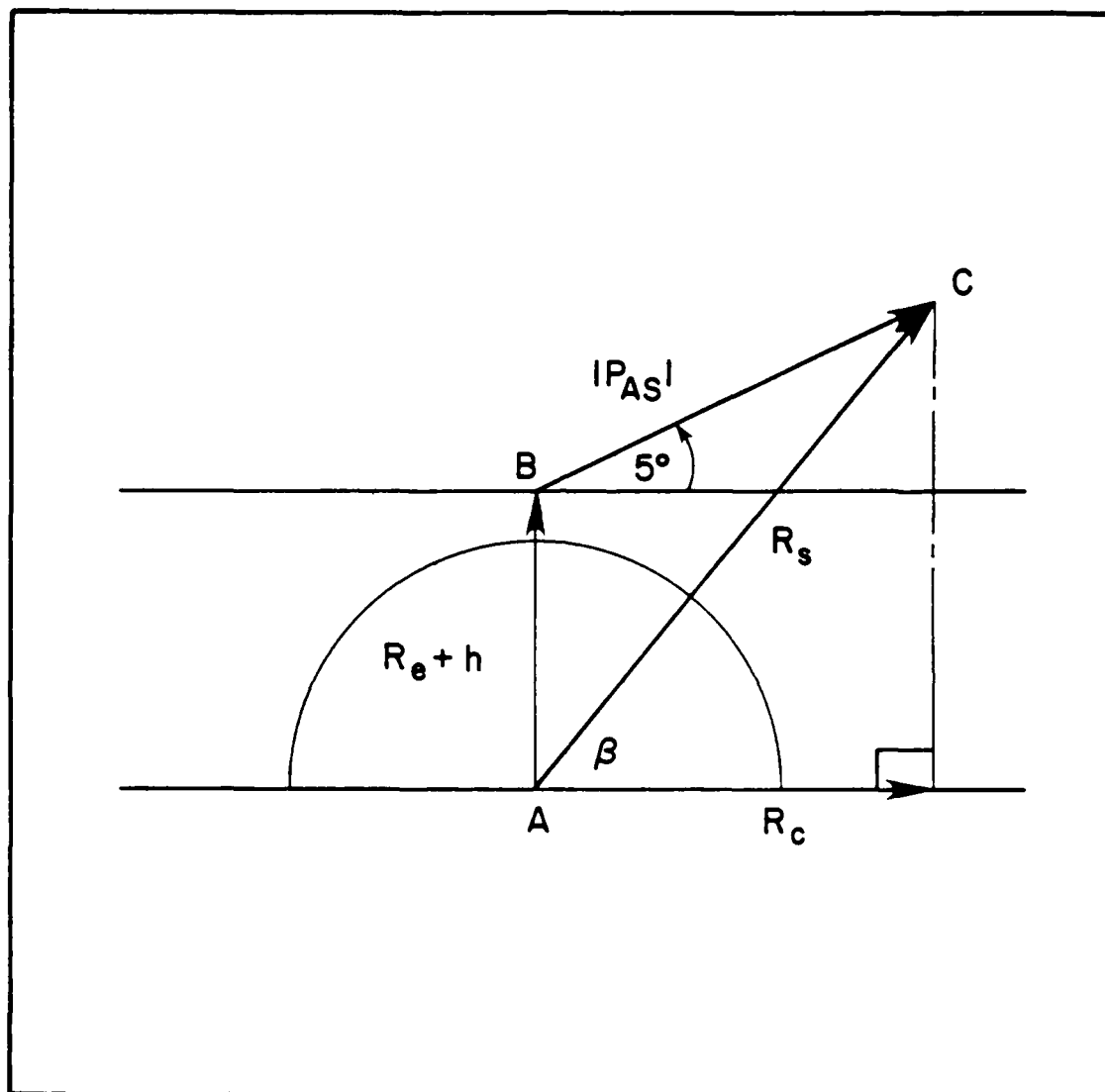


FIG. 3.1. GEOMETRY FOR LOS ELEVATION CONSTRAINT

$$C = \arcsin \left[ \frac{(R_e + h) \sin 95^\circ}{R_s} \right] \quad (3-30)$$

Now find  $\beta$

$$\beta = 90^\circ - A \quad (3-31)$$

where

$$A = 180^\circ - (B + C) \quad (3-32)$$

Substituting  $R_s = 8.4116 \times 10^7$  into Eqn (3-28) yields

$$|R_c| = 7.934 \times 10^7 \text{ feet} \quad (3-33)$$

This figure is now used to determine when projected satellite positions violate the LOS elevation constraint. If the satellite position projection violates this constraint, then it is reset onto the constraint boundary.

The actual cost gradient,  $\underline{g}(\underline{P}_s)$ , is developed in Appendix A. This cost gradient is now incorporated into a minimum cost search as described in the next section.

### 3.5 MINIMUM COST SEARCH TECHNIQUE

The search technique selected for minimizing the cost function in this study is a steepest descent algorithm. The

search scheme is based on the premise that the computed gradient  $\underline{g}(\underline{P}_s)$  indicates the direction of maximum rate of increase in the cost for a given  $\underline{P}_s$ . Therefore, the negative gradient direction must represent the direction of maximum rate of decrease in the cost. It is possible to proceed along the negative gradient direction until a minimum cost along this gradient is determined. At this point a new gradient direction is computed and search proceeds along the new negative gradient direction. The search continues until the gradient vector computed has a magnitude smaller than a preset threshold. The initial step size for the search is chosen by trial and error. It is important to consider the trade-offs between the number of intermediate points required to reach the minimum along a gradient direction and the possibility of grossly overshooting that minimum when determining the initial step size.

The minimum cost function point along a given gradient search direction  $\underline{g}_0$  is found by monitoring the angle condition between  $\underline{g}_0$  and  $\underline{g}_i$  using the cosine of the angle between the two vectors. This cosine is computed by using the definition of the inner product (or vector projection)

$$\langle \underline{g}_0, \underline{g}_i \rangle = | \underline{g}_0 | | \underline{g}_i | \cos \theta \quad (3-34)$$

where  $\theta$  is the angle between the two vectors.

Solving for  $\cos \theta$

$$\cos \theta = \frac{\langle \underline{g}_o, \underline{g}_i \rangle}{| \underline{g}_o | | \underline{g}_i |} \quad (3-35)$$

The minimum cost point along  $\underline{g}_o$  occurs where  $\underline{g}_i$  is orthogonal to  $\underline{g}_o$ , i.e. where  $\cos \theta = 0$ . When this orthogonality condition is met, the  $\underline{g}_i$  becomes the new  $\underline{g}_o$  and  $\underline{P}_{Si}$  becomes  $\underline{P}_{So}$  as shown in Fig. 3.2.

The vector  $\underline{P}_{Si}$  is computed as

$$\underline{P}_{Si} = \underline{P}_{So} + S_i \underline{g}_o \quad (3-36)$$

where

$$S_i = ( 1 + 0.9 \cos \theta_{i-1} ) S_{i-1} \quad (3-37)$$

Note that  $S_o$  is the initial step size selected and that the algorithm automatically reduces the step size as the  $\underline{g}_o$ ,  $\underline{g}_i$  orthogonality condition is approached.

This search algorithm is modified due to the fact that the satellites may move in either an unconstrained or constrained manner. Constrained movement is required when the gradient search direction indicates the satellite should be moved onto or beyond the  $R_c$  boundary. In this study, the constrained and unconstrained satellite movements are computed independently using separate initial step size parameters. Now,  $\underline{g}_o$  is given by

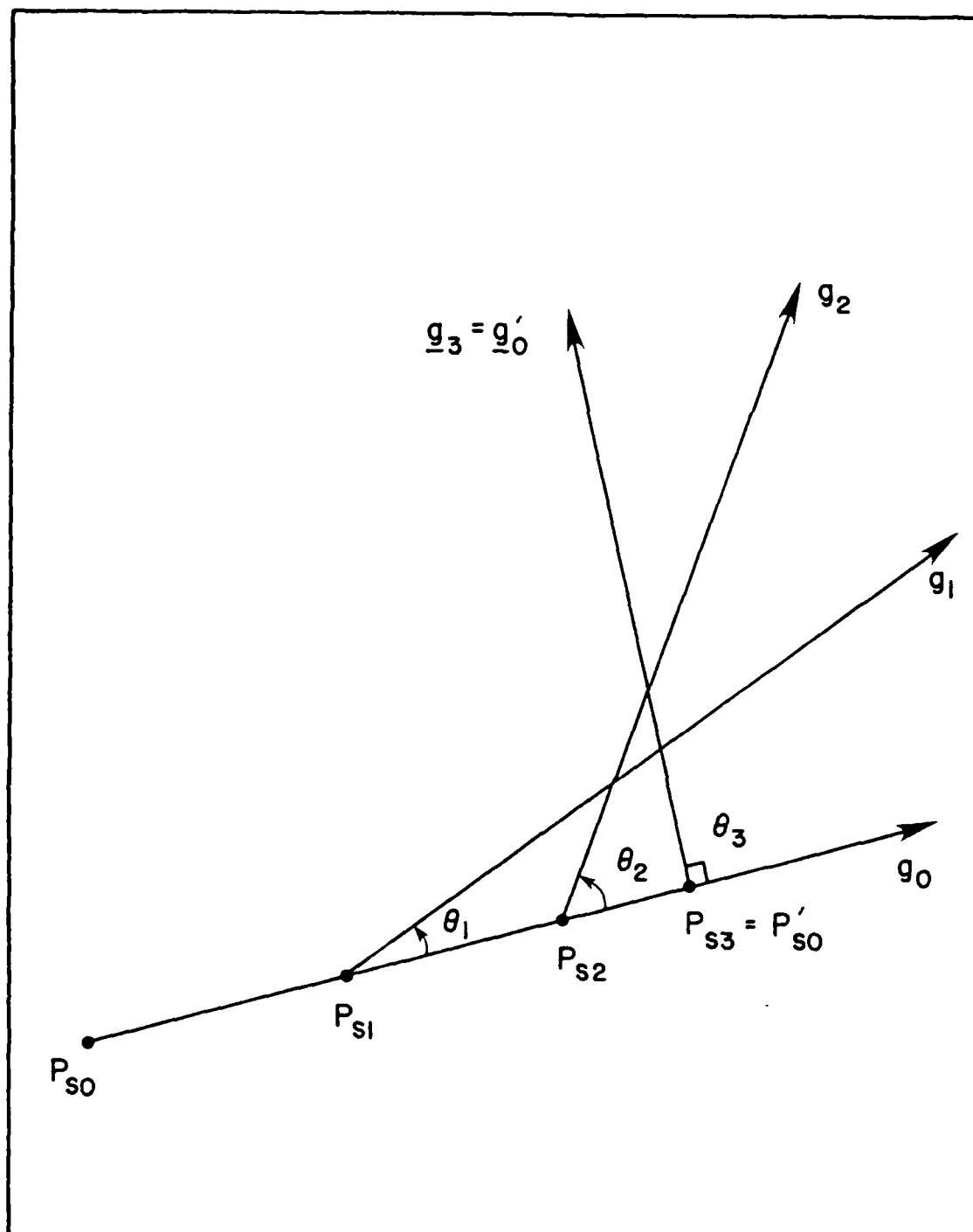


FIG. 3.2. STEEPEST DESCENT SEARCH TECHNIQUE

$$\underline{g}_0 = [\underline{g}_0]_{\text{CON}} + [\underline{g}_0]_{\text{UNCON}} \quad (3-38)$$

Whenever a satellite reaches the  $R_c$  boundary,  $\underline{g}_0$  is redefined and the search begins along the new gradient search direction. The  $[\underline{g}_0]_{\text{UNCON}}$  is simply redefined using  $\underline{g}_i$  for the satellites that have not reached the boundary and, similarly,  $\underline{P}_{Si}$  becomes  $\underline{P}_{So}$ . The  $[\underline{g}_0]_{\text{CON}}$  is actually the projection of  $\underline{g}_i$ , for the satellites on the boundary, onto a vector tangent to the boundary circle at  $\underline{P}_{Si}$ . This projection is done so that, in approximation, gradient search is done along the circular boundary as indicated in Fig. 3.3. If, during gradient search along the boundary,  $\underline{g}_i$  indicates satellite movement should be off the boundary, then  $\underline{g}_0$  is again reset such that the appropriate satellite may move off the boundary constraint.

To find  $[\underline{g}_0]_{\text{CON}}$  first define the normal vector at  $\underline{P}_{Si}$  for the  $j$ -th satellite

$$\underline{n} = [y_j, z_j] \quad (3-39)$$

The tangent vector at  $\underline{P}_{Si}$  is then

$$\underline{t} = [z_j, -y_j] \quad (3-40)$$

which is normalized to form the unit tangent vector

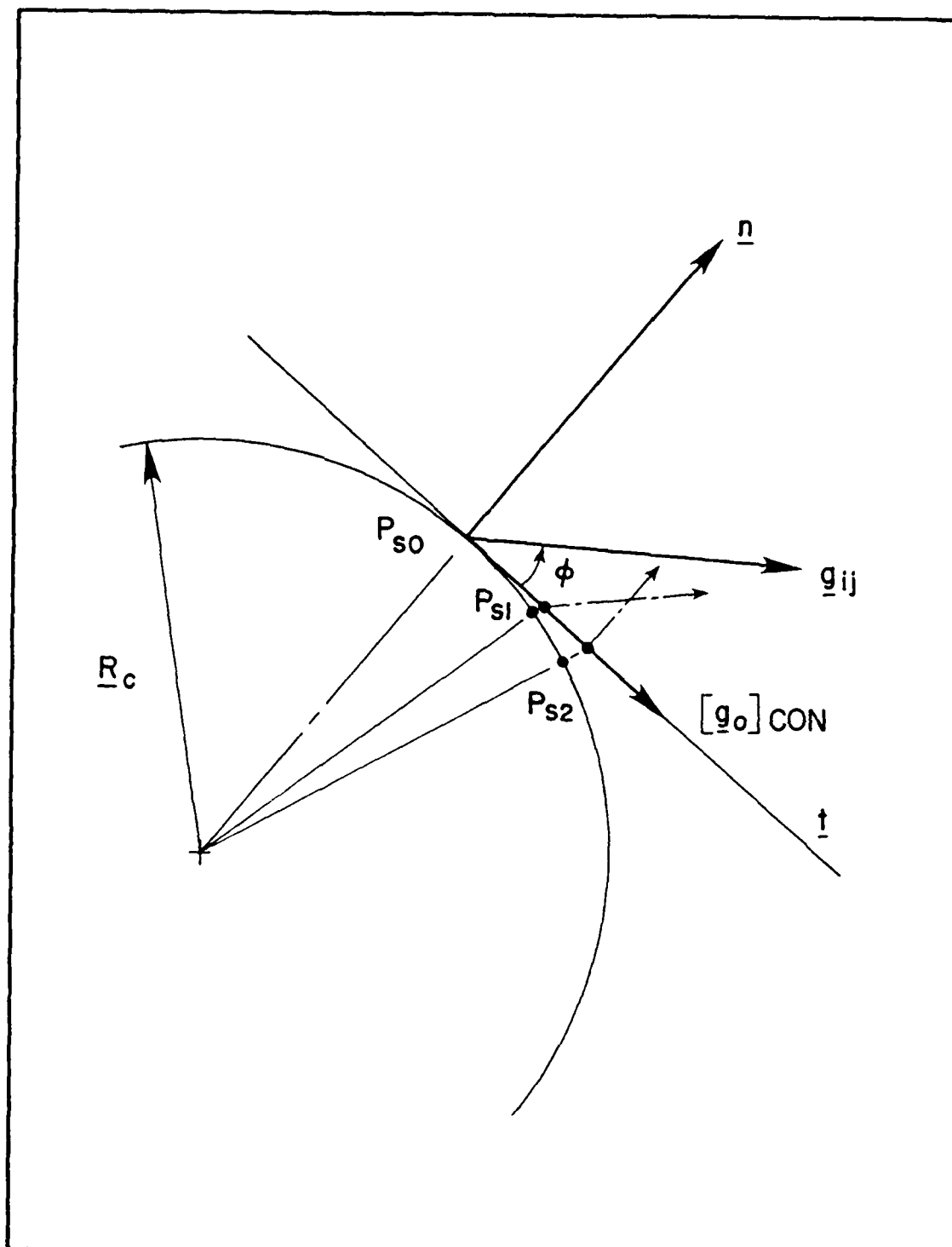


FIG. 3.3. PROJECTION OF GRADIENT ONTO TANGENT

$$\underline{u}_t = [u_{zj} , u_{yj}] \quad (3-41)$$

The projection angle  $\phi$  is given by

$$\cos \phi = \frac{\langle \underline{g}_{ij} , \underline{u}_t \rangle}{| \underline{g}_{ij} |} \quad (3-42)$$

The projection magnitude is computed as

$$| [\underline{g}_o]_{\text{CON}} | = | \underline{g}_{ij} | \cos \phi \quad (3-43)$$

Finally,  $\underline{g}_o$  for the constrained satellite is given as

$$[\underline{g}_o]_{\text{CON}} = | [\underline{g}_o]_{\text{CON}} | \underline{u}_t \quad (3-44)$$

The termination condition for search in the case of constrained satellites can obviously no longer be based on the magnitude of the computed gradient vector being small. The appropriate termination condition in this case is when the computed gradient vector is orthogonal to the tangent vector or, in other words, when the projection of the gradient vector onto the tangent is very nearly zero.

Having developed the basic mechanisms for estimation, cost function computation, and minimum cost search, the analysis is accomplished. The next chapter reports the results.

## IV. RESULTS

### 4.1 INTRODUCTION

In this study, the work accomplished by Lewantowicz in his December 1985 Master of Science thesis (4) is expanded and used as a starting point for further research. In particular, the effect of iterating the error covariance matrix to steady state after each satellite repositioning movement is examined. This chapter examines the optimum positions of GPS satellites for the four, three, and two satellite cases such that minimum errors in the estimate of emitter location are made. The results of the four and three satellite cases are compared directly with the results obtained by Lewantowicz. In addition, the validity of using a fourth satellite directly overhead to simulate a three satellite case where each observer has a precise clock is examined. The performance of the emitter location system is evaluated for each optimum satellite configuration and the results are compared.

Using the satellite geometry relations to the cost data obtained in all the optimization runs, the basic guidelines are developed for a satellite selection algorithm formulation. The factors considered in forming the algorithm, as well as justifying data, are presented in section 4.5.

#### 4.2 FOUR SATELLITE OPTIMIZATION

The four satellite position optimization problem begins with the SVs and observers in the initial configuration shown in Fig. 4.1. These positions were selected to correspond with those used by Lewantowicz so that a direct comparison can be made. Note not only the initial geometry of the problem, but also the characteristics of each of the error ellipses. Each observer error ellipse has a particular size and orientation, and the emitter error ellipse has important characteristics of size and elongation, which are ultimately reflected in the CEP. It should be pointed out that the elongation of the emitter error ellipse, in general, is not taken into account if the chosen satellite geometry only minimizes the observer navigation problem. For many practical applications, the orientation and elongation of the emitter error ellipse is of critical importance, especially in the case of highly elongated ellipses. The initial satellite position data is given in Table 4.1 and initial error ellipse parameters are presented in Table 4.2.

From this starting point, the goal is to accomplish a gradient search which will move the satellites to an orientation yielding minimum emitter MSMD (and CEP). However, before each of the gradient computations is performed, it is desirable to iterate the error covariance matrix to steady-state at a constant SV position to examine the Kalman filter convergence time history.

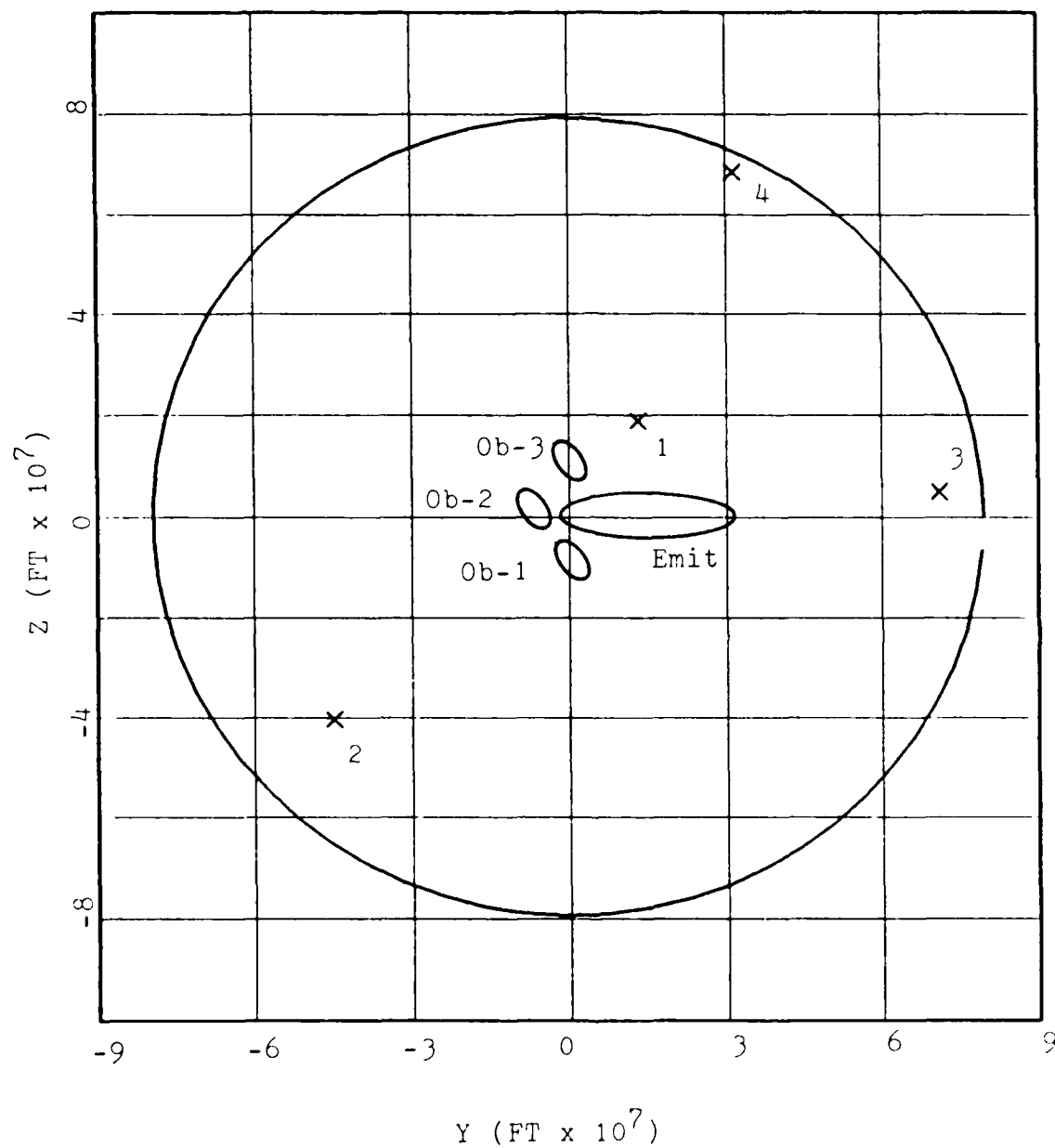


Fig. 4.1. Four Satellite Initial Configuration

Table 4.1. Four Satellite Initial Positions

	<u>Azimuth (<math>^{\circ}</math>)</u>	<u>Elevation (<math>^{\circ}</math>)</u>	<u>LOS Bias (ft)</u>
SV-1	35.0	69.0	9.8
SV-2	228.0	31.9	9.6
SV-3	86.0	18.6	10.7
SV-4	24.6	12.2	9.7

Table 4.2. Four Satellite Initial Error Ellipse Parameters

	<u>Axis 1 (ft)</u>	<u>Axis 2</u>	<u>Angle from Y (<math>^{\circ}</math>)</u>	<u>CEP (ft)</u>
Obs-1	16.4	8.7	-49.8	14.8
Obs-2	16.4	8.7	-49.9	14.8
Obs-3	16.3	8.8	-49.9	14.8
Emit	82.5	16.1	0.21	58.0

Although many methods exist to determine the number of iterations required to reach steady-state operation, this study examined the relationship between the number of iterations of the error covariance matrix and the parameters describing the emitter error ellipse. In particular, the change in magnitude of CEP,  $\Delta\text{CEP}$ , from iteration  $i$  to  $i+1$  is computed and the minimum value is sought as a function of  $i$ . In addition, the convergence angle, which is the angle between the gradient vector computed at iteration  $i$  and the gradient vector at iteration  $i+1$ , is monitored to determine when the computed gradient vectors become coaligned. The  $\Delta\text{CEP}$  for 200 Kalman filter iterations of the error covariance matrix propagation and update is presented in Fig. 4.2. Note the rapid drop in CEP improvement as the iterations increase, with a local minimum occurring at eight iterations. This minimum is clearly shown on the expanded iteration scale in Fig. 4.3. The behavior of  $\Delta\text{CEP}$  after iteration eight is presented on an expanded  $\Delta\text{CEP}$  scale in Fig. 4.4. Note the transient dynamic behavior of the matrix Ricatti equation solution as reflected by this CEP measure in Fig. 4.4, and the second local minimum at approximately 35 iterations. From the data presented, the obvious choice for the number of iterations of the error covariance matrix to use for steady state would be one of the two local minima. Due to the computational loading required to propagate and update the error covariance matrix at each cost function search point, and the magnitude of improvement expected with increased iterations, the

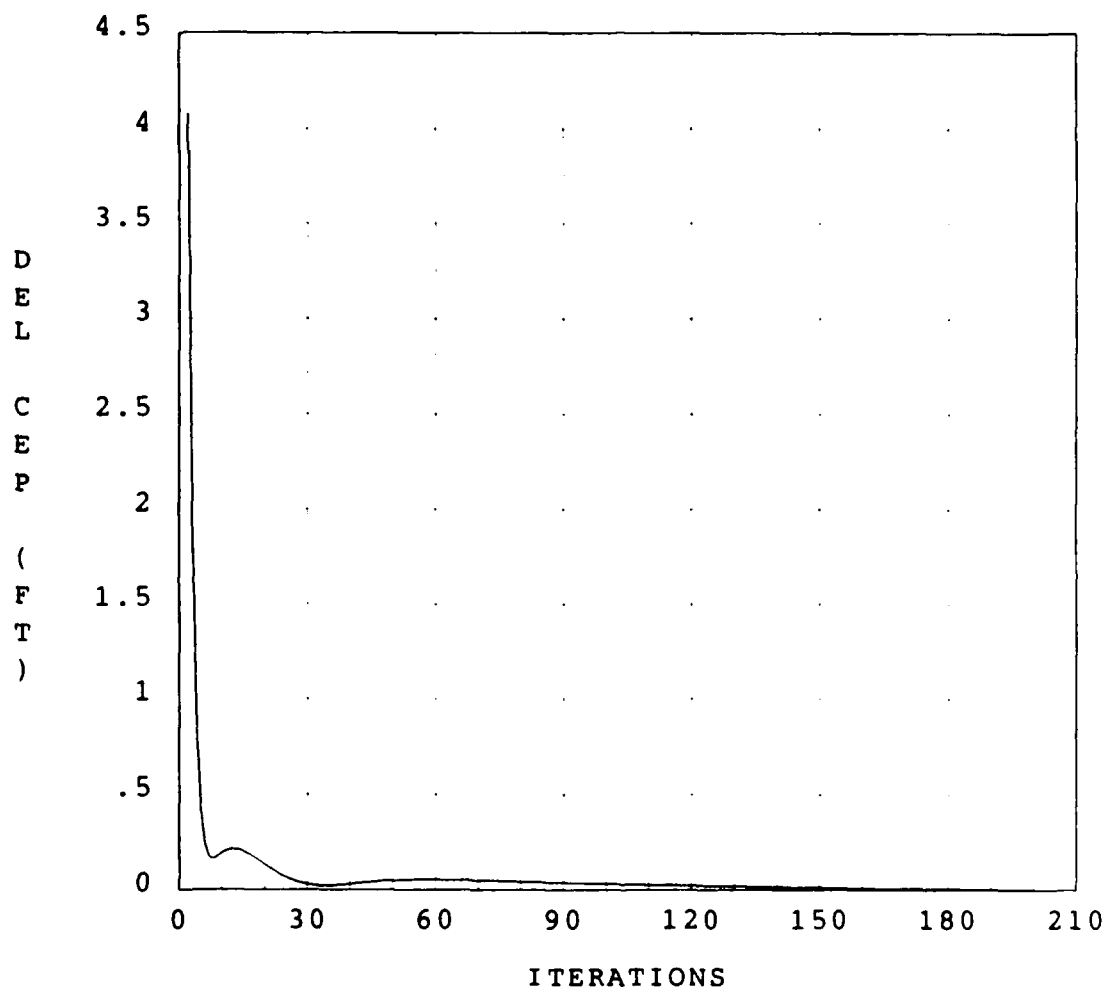


Fig. 4.2. CEP Behavior During Filter Iterations

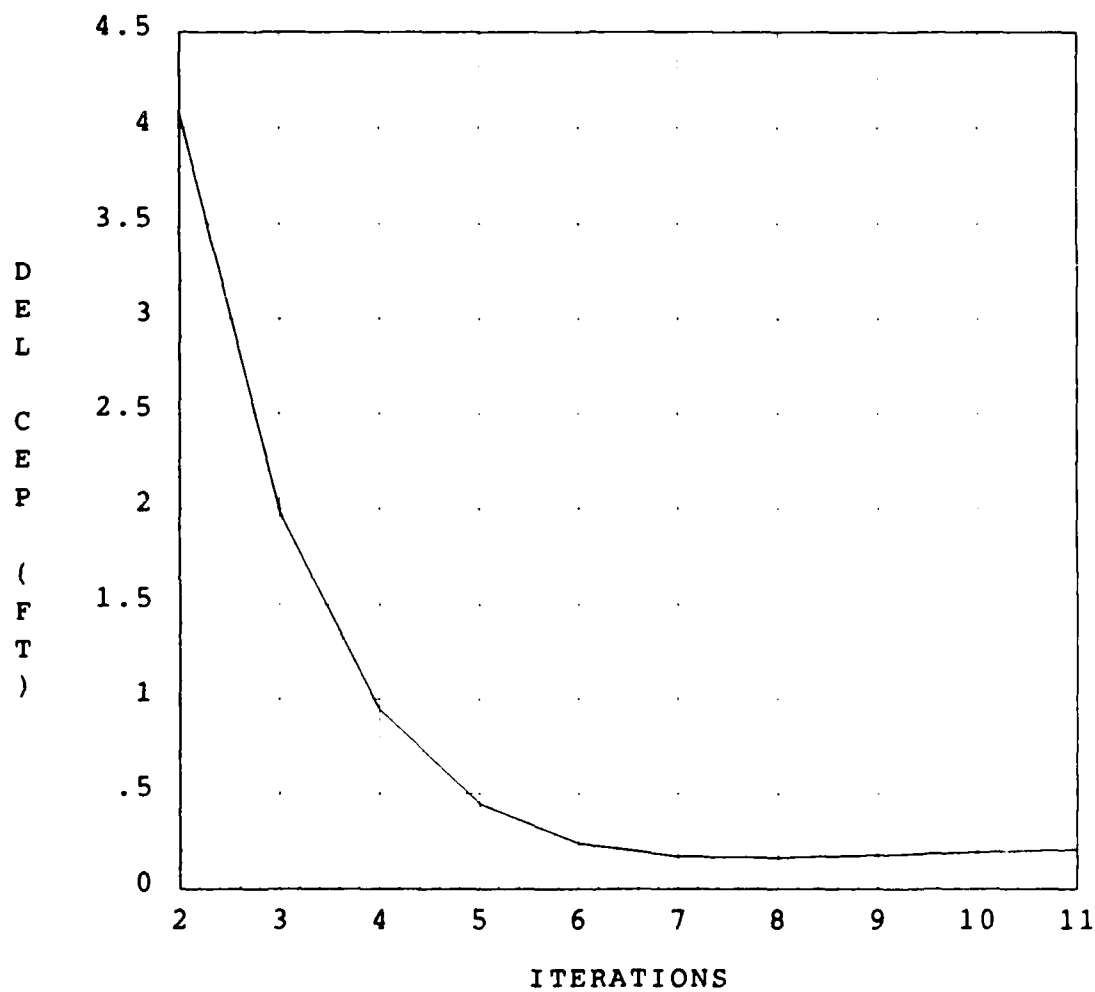


Fig. 4.3. CEP Behavior at First Local Minimum

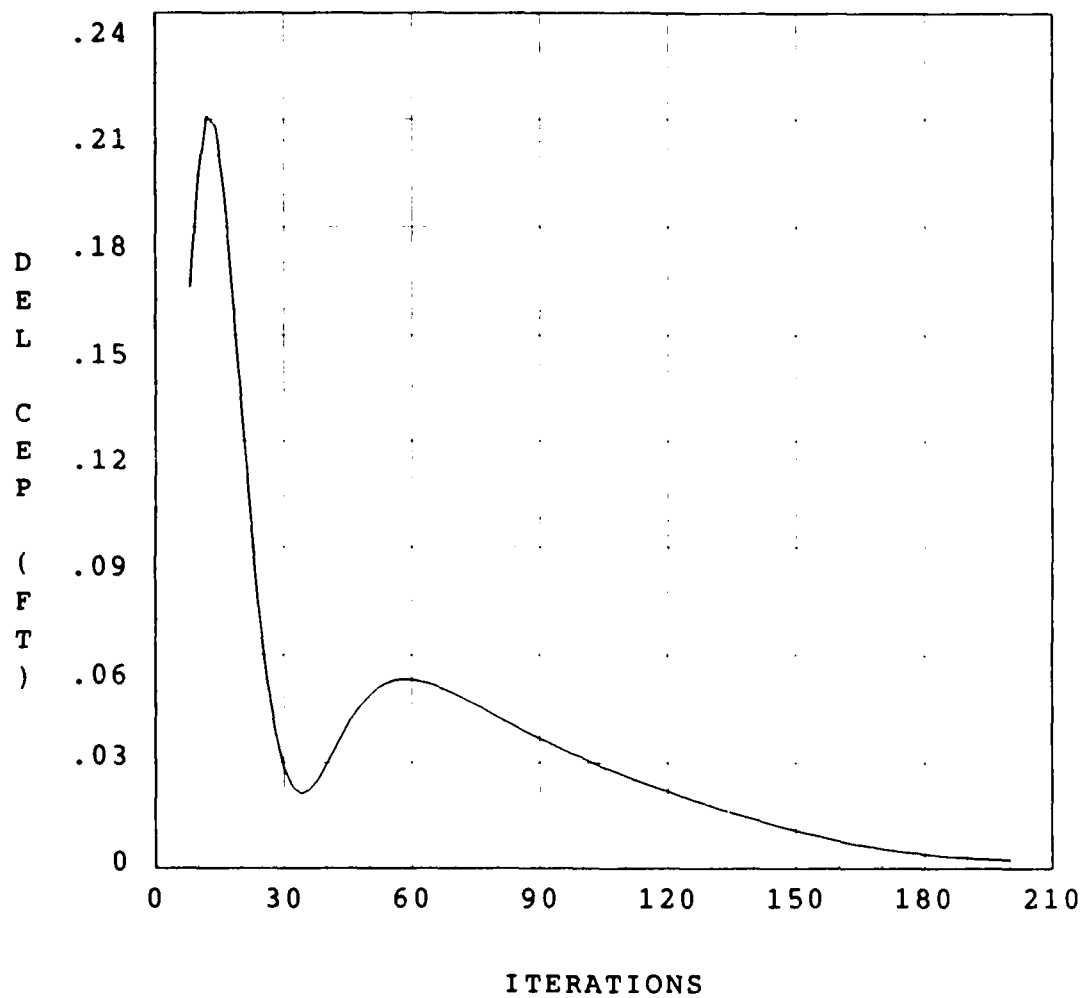


Fig. 4.4. CEP Transient Behavior

local minimum of eight iterations was selected to approximate steady-state operation for this study. Gradient vector convergence at 8 iterations is good, with a convergence angle of less than 0.6 degrees. With eight iterations established as the number of iterations prior to each gradient vector computation, the minimum cost search for the four satellite case is conducted. Note that the eight iteration figure was obtained with the satellites and observers only at their initial positions. Therefore, this figure may or may not be appropriate for all possible scenarios.

The satellite positions determined by the minimum cost search are presented graphically in Fig. 4.5, with position data and error ellipse parameters given in Tables 4.3 and 4.4, respectively. The paths the satellites "traveled" during the gradient search in reaching their final positions are shown in Fig. 4.6. The minimum emitter CEP found is 41.22 feet, down from the initial CEP of 58.0 feet. Comparing Tables 4.2 and 4.4, it can be seen that the observer horizontal navigation errors have been significantly reduced. This reduction results from a marked decrease in LOS bias errors as indicated in Table 4.3. The reduction in these east-west observer navigation errors directly affect the shape and orientation of the emitter ellipse. In fact, these reductions are the driving force behind the reduction in the semi-major axis of the emitter ellipse and, ultimately, the emitter CEP. Note that three of the four

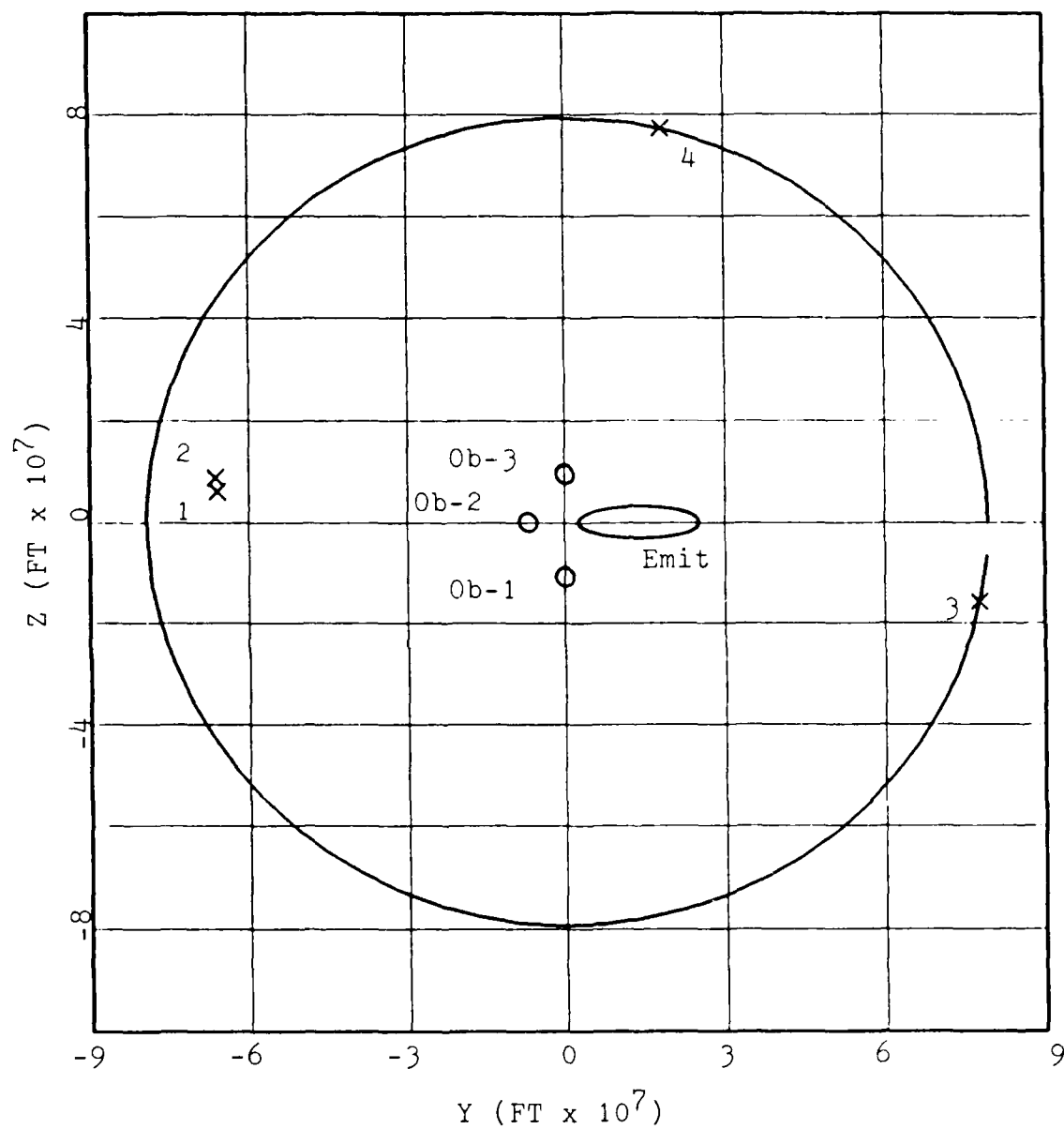


Fig. 4.5. Four Satellite Final Configuration

Table 4.3. Four Satellite Final Positions

	<u>Azimuth (<math>^{\circ}</math>)</u>	<u>Elevation (<math>^{\circ}</math>)</u>	<u>LOS Bias (ft)</u>
SV-1	275.3	25.0	2.8
SV-2	277.4	24.3	2.9
SV-3	101.5	5.0	2.6
SV-4	13.3	5.0	1.8

Table 4.4. Four Satellite Final Error Ellipse Parameters

	<u>Axis 1 (ft)</u>	<u>Axis 2</u>	<u>Angle from Y (<math>^{\circ}</math>)</u>	<u>CEP (ft)</u>
Obs-1	3.15	2.02	-41.5	3.04
Obs-2	3.16	2.02	-42.0	3.05
Obs-3	3.00	1.77	-35.5	2.81
Emit	62.98	7.05	- 0.07	41.22

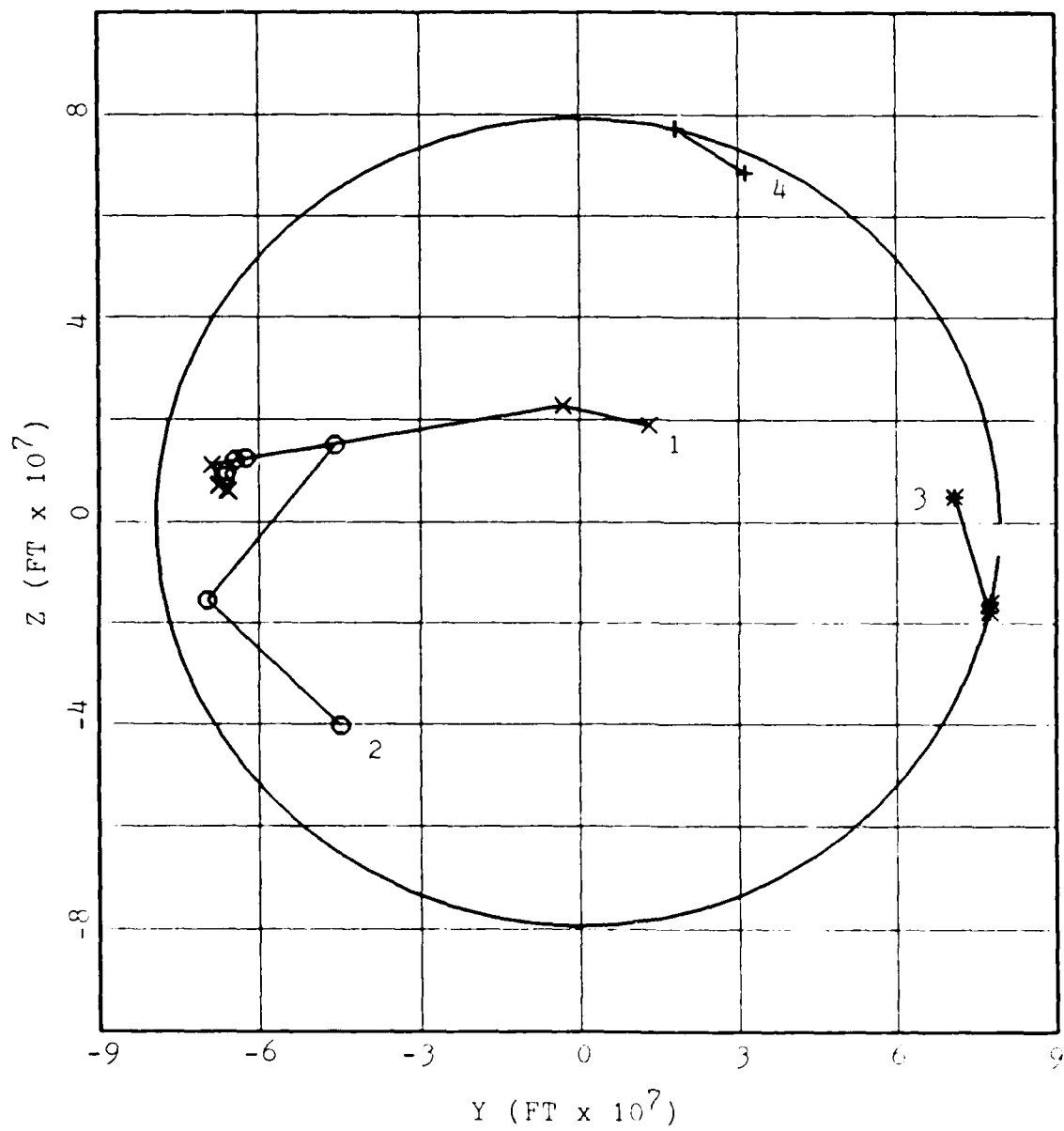


Fig. 4.6. Four Satellite Trajectory

satellites tended to align themselves along the east-west axis in opposition to each other. This alignment produced the noted reductions in the east-west emitter location error, and reflects the type of optimum geometry expected at the outset of this study. The fact that the semi-major axis of the emitter error ellipse lies along the east-west axis is a function of the observer geometry.

Comparing the results of the four satellite optimization with those obtained by Lewantowicz (4) indicates that the satellite positions are within  $10^\circ$  of each other in azimuth and elevation and the minimum emitter CEPs are within two feet of one another. This supports the Lewantowicz hypothesis described in Section 1.5. Next, the three satellite optimization is performed.

#### 4.3 THREE SATELLITE OPTIMIZATION

As pointed out in Section 3.3, the cost function used in this study was formulated for an essentially two-dimensional problem. This means that the problem is uniquely solved with only three satellites and the fourth satellite only provides additional horizontal emitter position information. The performance of the emitter locating system is evaluated for two separate three satellite cases; first, one satellite is fixed overhead and three satellites are allowed to move (see Section

1.5) and, second, the measurements from only three satellites are incorporated into the error covariance computation.

The "pseudo" three satellite case, as proposed by Lewantowicz (4) uses four satellites with one fixed directly overhead and is intended to simulate the three satellite case when each observer has a precise clock. The results of the pseudo-three satellite optimization are presented in Fig. 4.7 and Tables 4.5 and 4.6. The paths the satellites "traveled" in reaching their final positions are shown in Fig. 4.8. Note the final CEP achieved in the pseudo-three satellite case is 40.71 feet compared to 41.22 feet obtained in the four satellite case. These results seem unreasonable since they indicate that the CEP improved when less position information was available. What has happened is that a three satellite optimization has not been performed, but, rather, a constrained four satellite case has been optimized. The gradient search performed for the constrained satellite case found a different local minimum than that found in the original four satellite case. The existence of this second local minimum indicates that finding a global minimum using the gradient search algorithm of this study is highly unlikely. However, the magnitude of the second local minimum varies only slightly from the first minimum, indicating that it is reasonable to expect other local minima to result in nearly the same costs. Note that satellites 1 and 2 in the pseudo-three satellite case have assumed approximately the same

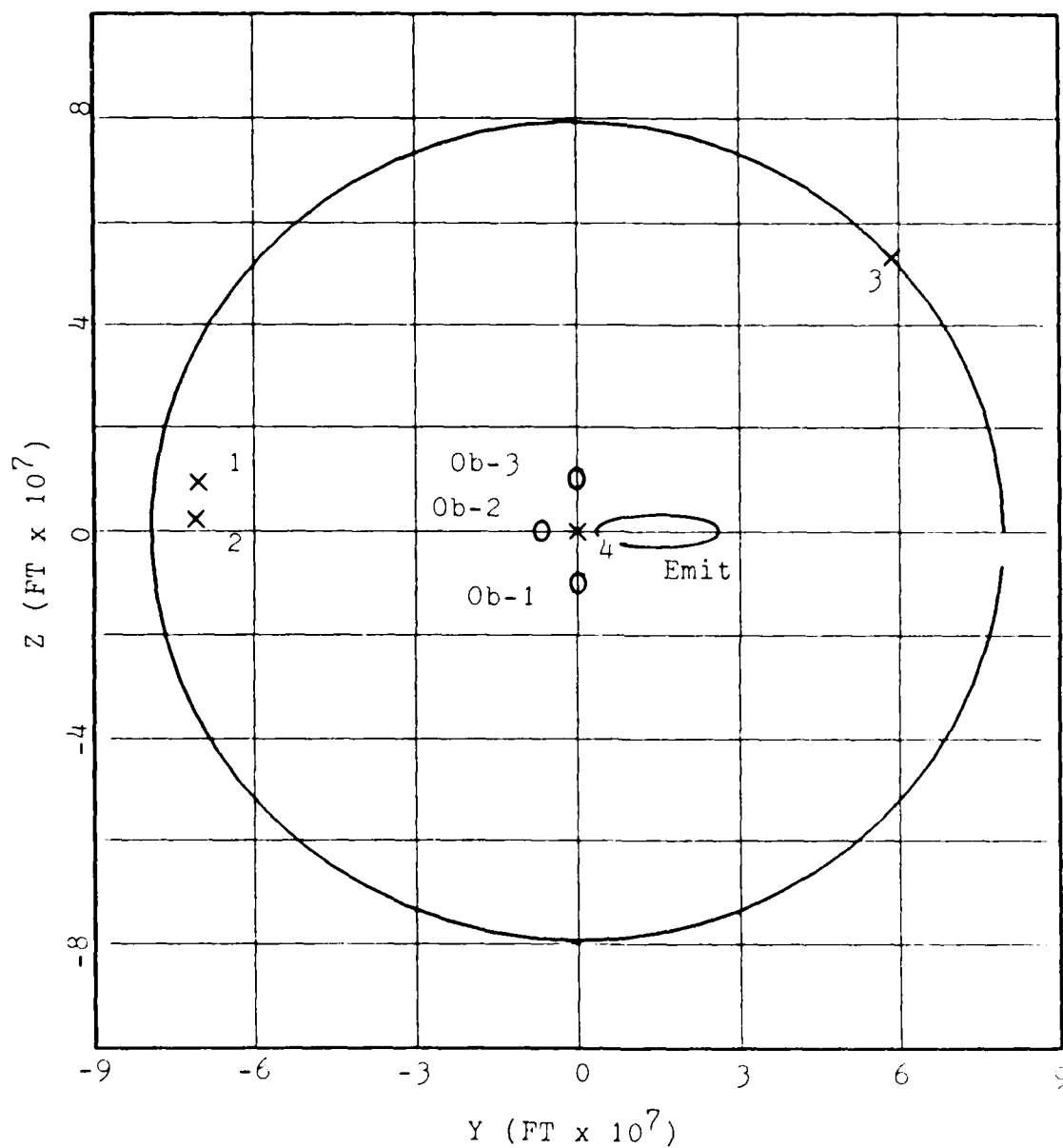


Fig. 4.7. Pseudo Three Satellite Final Geometry

Table 4.5. Pseudo Three Satellite Final Positions

	<u>Azimuth (<math>^{\circ}</math>)</u>	<u>Elevation (<math>^{\circ}</math>)</u>	<u>LOS Bias (ft)</u>
SV-1	277.4	16.7	1.6
SV-2	272.3	17.1	1.7
SV-3	47.7	5.0	1.6

Table 4.6 Pseudo Three Satellite Error Ellipse Parameters

	<u>Axis 1 (ft)</u>	<u>Axis 2</u>	<u>Angle from Y (<math>^{\circ}</math>)</u>	<u>CEP (ft)</u>
Obs-1	2.46	1.55	-88.0	2.34
Obs-2	2.50	1.54	-87.7	2.38
Obs-3	1.74	1.35	65.1	1.82
Emit	62.33	6.82	- 0.01	40.71

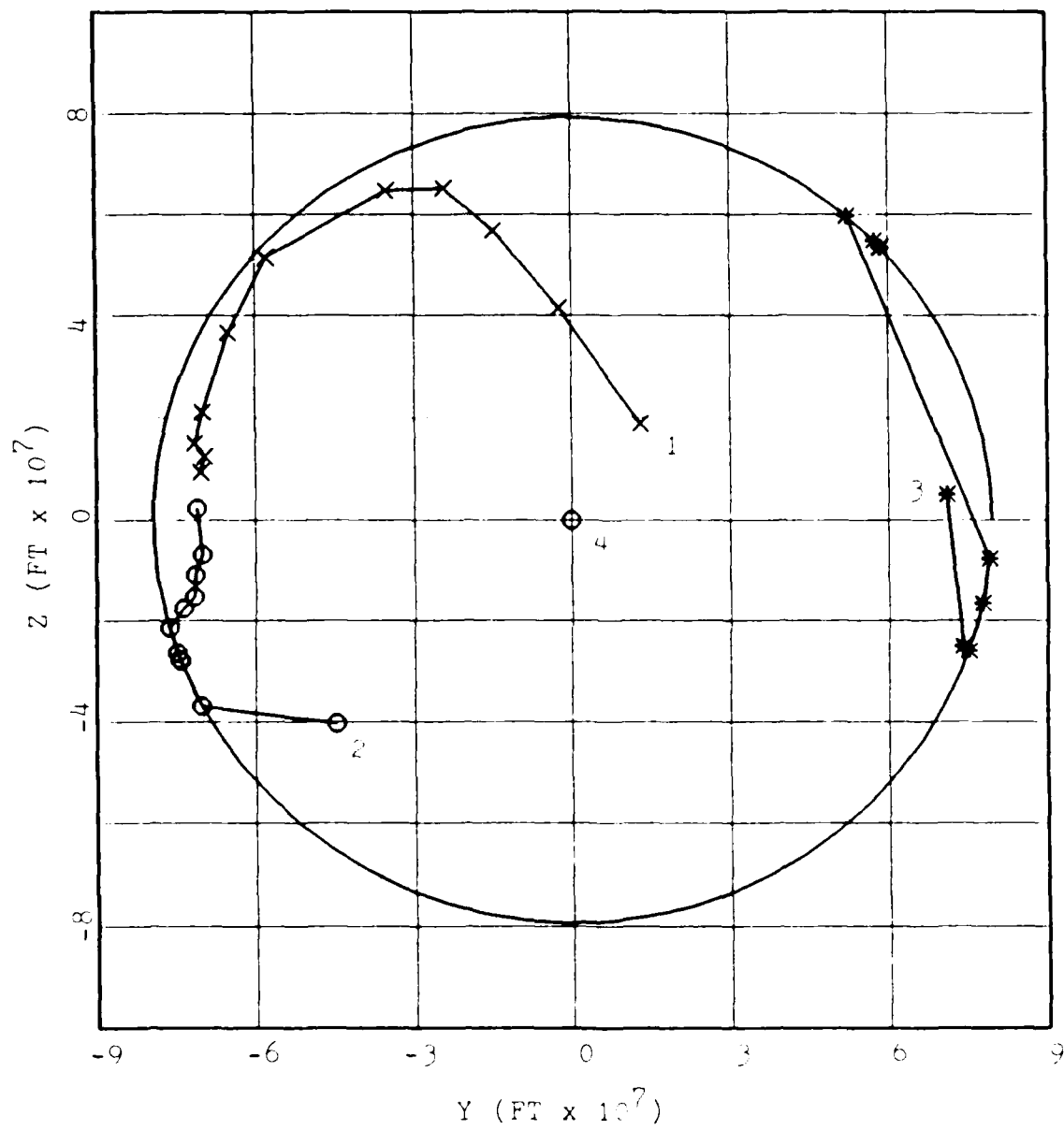


Fig. 4.8. Pseudo Three Satellite Trajectory

positions that they did in the four satellite case, adding credence to the idea of a constrained four satellite case.

The fact that the pseudo-three satellite optimization yields better results than the four satellite case indicates that the simulation of a three satellite case using four satellites, with one satellite fixed overhead, is not appropriate. This is further verified by the following true three satellite optimization.

For the true three satellite case, the measurements from only three satellites are incorporated in the error covariance matrix. The three satellite optimization results are given in Fig. 4.9 and Tables 4.7 and 4.8. Again, satellite tracks are indicated in Fig. 4.10.

The results in Table 4.8 are reasonable for the three satellite case, with the CEP of 43.01 feet slightly higher than the CEP of 41.22 feet obtained in the four satellite analysis, as expected. This is because the problem is essentially planar and three satellites are sufficient to determine position and user clock bias states. The barometric altimeter still stabilizes the INS vertical channel, but the large vertical position errors do not affect the planar emitter location problem. Note that the optimum satellite positions in the true three satellite case are considerably different from those

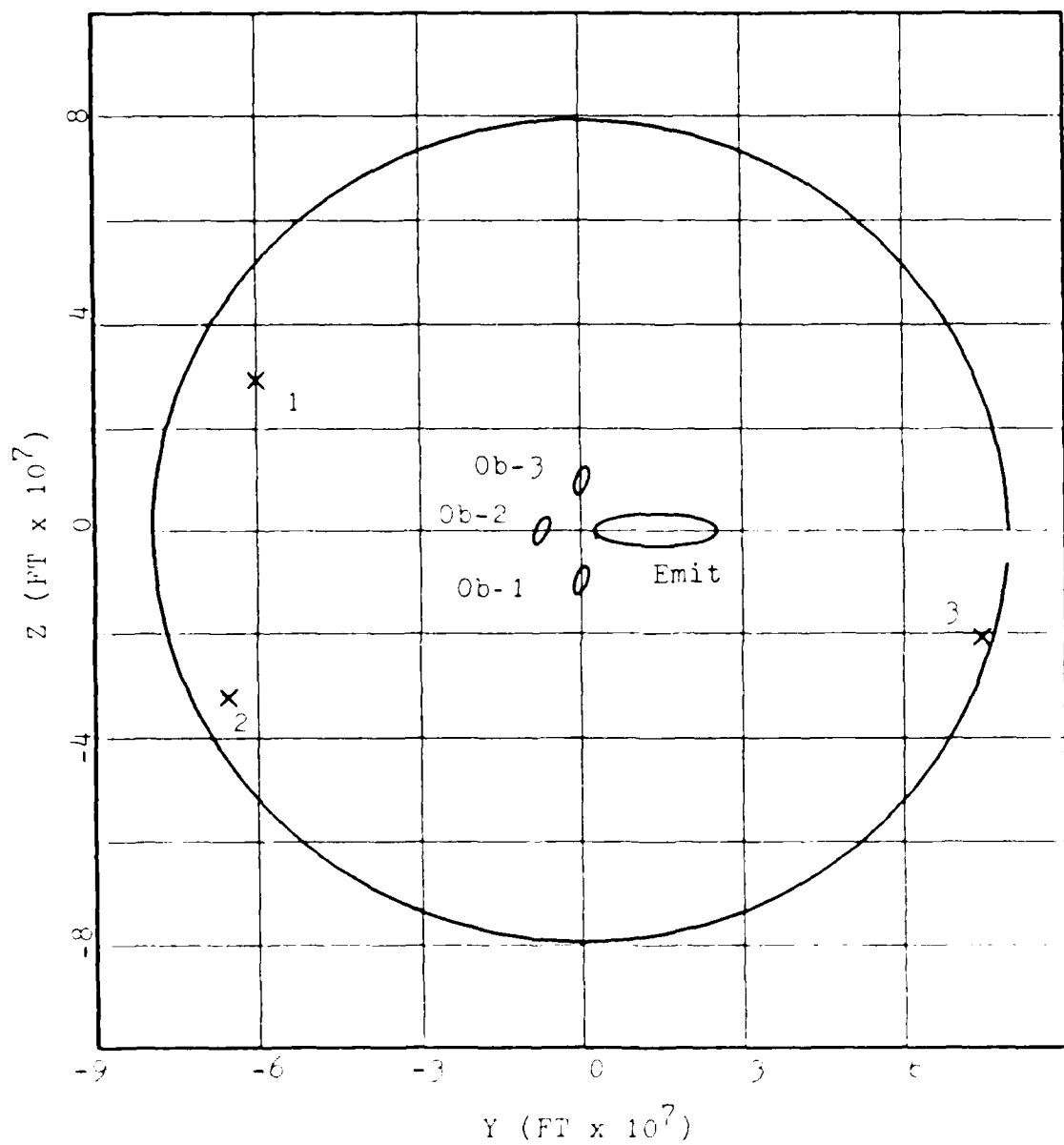


Fig. 4.9. Three Satellite Final Geometry

Table 4.7. Three Satellite Final Positions

	<u>Azimuth</u> ( $^{\circ}$ )	<u>Elevation</u> ( $^{\circ}$ )	<u>LOS Bias</u> (ft)
SV-1	299.6	22.4	3.1
SV-2	244.6	11.8	4.5
SV-3	105.9	9.3	3.7

Table 4.8. Three Satellite Error Ellipse Parameters

	<u>Axis 1</u> (ft)	<u>Axis 2</u>	<u>Angle from Y</u> ( $^{\circ}$ )	<u>CEP</u> (ft)
Obs-1	6.00	3.57	62.8	5.64
Obs-2	5.99	3.61	62.5	5.65
Obs-3	5.51	3.51	59.8	5.31
Emit	64.62	8.44	- 0.12	43.01

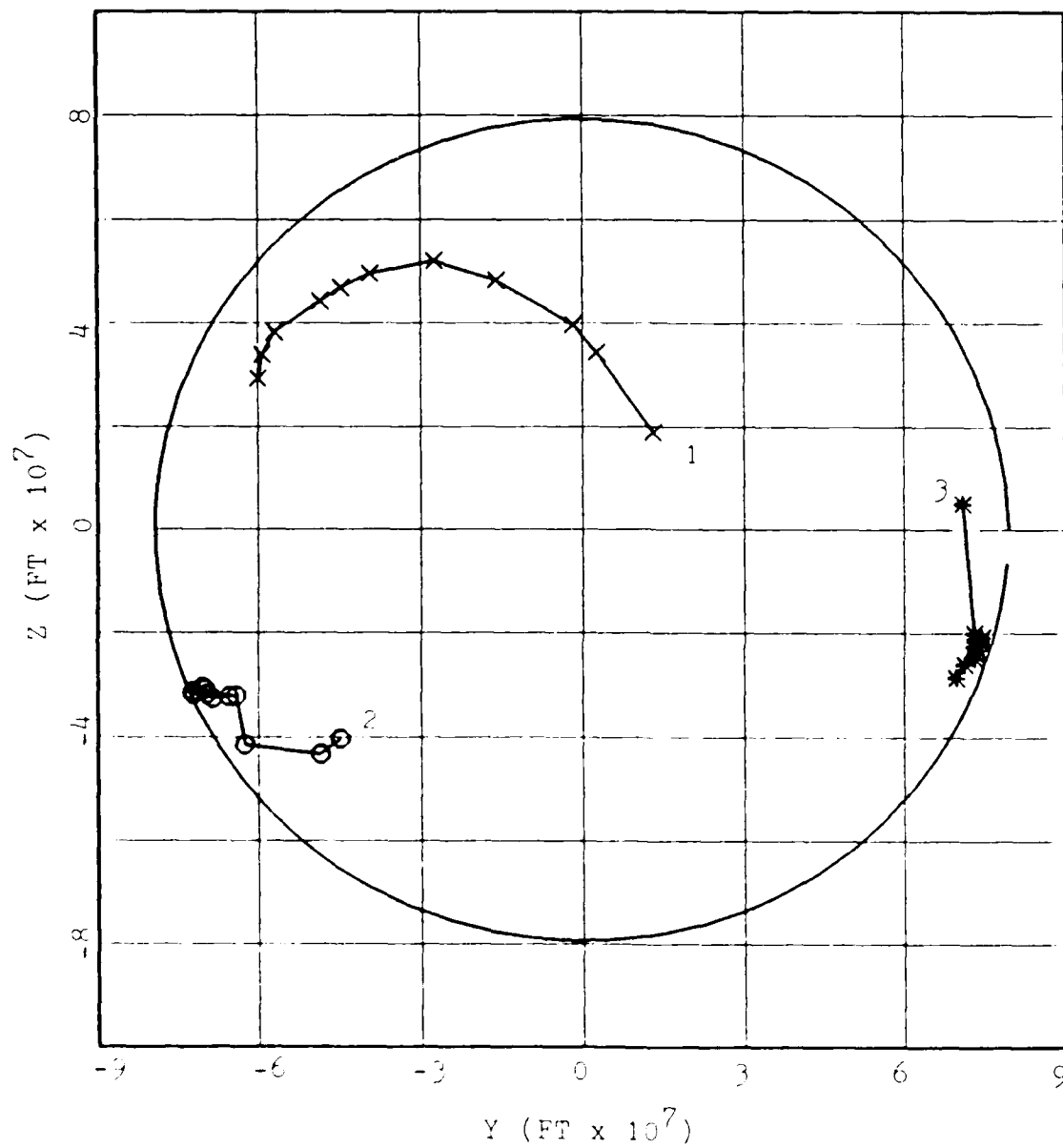


Fig. 4.10. Three Satellite Trajectory

obtained in the pseudo-three satellite optimization. The true three satellite optimization yields satellite positions which correspond to those anticipated at the outset of this study. SV-1 and SV-3 have assumed positions such that they reduce observer position errors primarily in the east-west direction and have also essentially aligned themselves so that LOS bias errors are reduced. This can be seen in Table 4.7 where SV-1 and SV-3 have the smaller LOS bias terms. SV-2 has taken up a position which is nearly symmetric with SV-1 about the east-west axis.

#### 4.4 TWO SATELLITE OPTIMIZATION

Again, as in the three satellite optimization, only measurements from the appropriate number of satellites are used in computing the error covariance matrix updates. This presents a problem in the two satellite case since, in general, three SVs are required to solve for a two-dimensional position and user clock bias. For the two satellite case in this study, the navigation filter is iterated to steady-state using measurements from four available SVs before operation is degraded to two satellites. This allows the Kalman filter to converge on accurate estimates of user clock bias and user clock drift states before degraded operation begins. Using these state estimates makes it possible to propagate the user clock bias forward with sufficient accuracy for some period of time.

The gradient search scheme converges on the optimum satellite configuration more quickly for the two satellite case than in the searches with more SVs. This is due in part to the fact that both satellites move onto the five degree constraint boundary and remain there. The optimization results are presented in Fig. 4.11 and Tables 4.9 and 4.10. Satellite paths to the optimum positions are shown in Fig. 4.12.

Note that for the two satellite case, SV-2 has again aligned itself along the east-west axis to provide maximum information along the long axis of the emitter error ellipse. Additionally, SV-1 has assumed a position that provides essentially the same amount of information in the y and z directions. The increase of approximately 13 to 15 feet in emitter CEP over the previous cases is reasonable since the system is depending upon filter estimates for user clock bias. It is significant to note, however, that the system is able to achieve good performance for some period of time, even when only two satellites are available for measurements.

The satellite geometry data obtained in the previous optimization cases is now used to develop a satellite selection algorithm that will minimize emitter CEP.

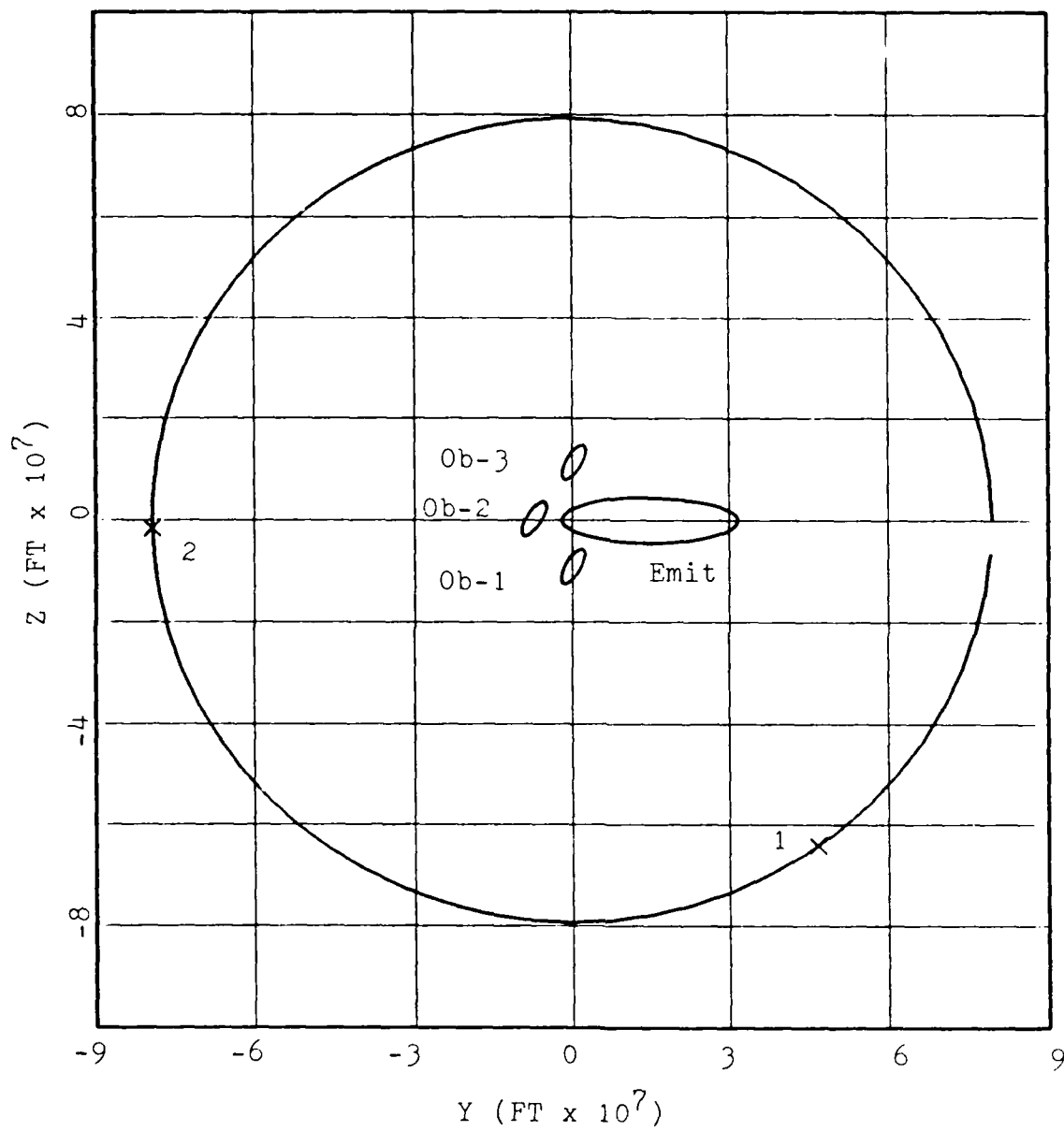


Fig. 4.11. Two Satellite Final Geometry

Table 4.9. Two Satellite Final Positions

	<u>Azimuth</u> ( $^{\circ}$ )	<u>Elevation</u> ( $^{\circ}$ )	<u>LOS Bias</u> (ft)
SV-1	143.9	5.0	1.80
SV-2	268.8	5.0	1.82

Table 4.10. Two Satellite Error Ellipse Parameters

	<u>Axis 1</u> (ft)	<u>Axis 2</u>	<u>Angle from Y</u> ( $^{\circ}$ )	<u>CEP</u> (ft)
Obs-1	13.53	2.96	66.6	9.70
Obs-2	12.83	2.98	60.7	9.30
Obs-3	14.92	2.97	60.6	10.54
Emit	82.95	12.66	0.89	56.28

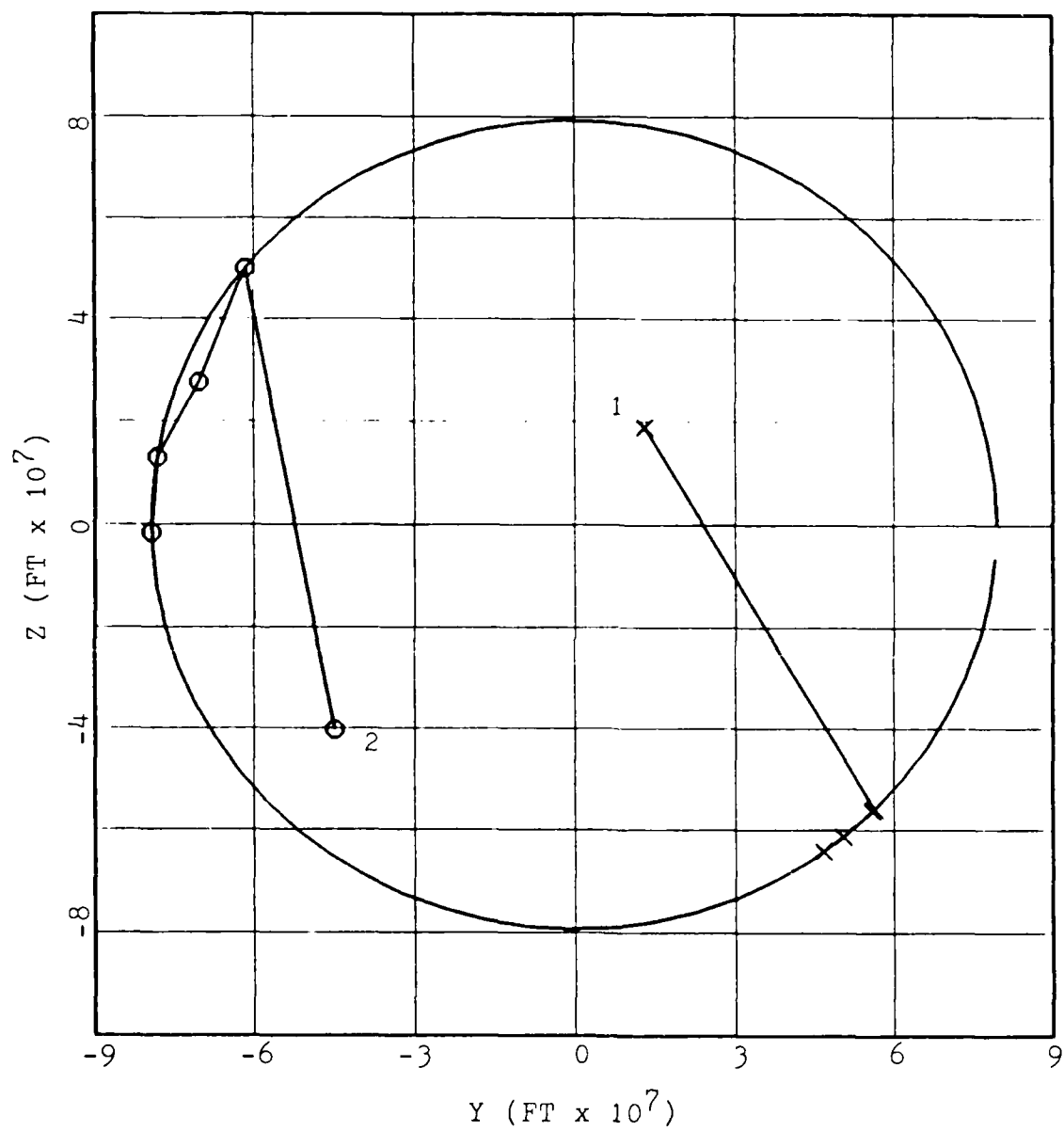


Fig. 4.12. Two Satellite Trajectory

#### 4.5 SATELLITE SELECTION ALGORITHM

When developing a satellite selection algorithm, there is a tradeoff between making the selection criteria restrictive enough to provide acceptable emitter CEPs and liberal enough to allow a wide range of possible satellite solution geometries. The basic approach used in this study is to examine the sensitivity of the emitter CEP to variations in satellite position from the optimum.

The previous optimization results indicate that the primary satellite(s) should be aligned along the semi-major axis of the emitter error ellipse. In addition, if more than two satellites are available, the primary satellites tend to lie along essentially the same LOS. Comparison of the different optimization results is useful to show trends in solution geometry. These trends are very useful in developing selection criteria. The final satellite positions for the four satellite optimization in Fig. 4.5 show SV-1 and SV-2 very close to alignment with the semi-major axis of the emitter error ellipse and along the same LOS as SV-3. Note that SV-4 is positioned to provide information primarily along the direction of the semi-minor axis of the emitter error ellipse. Comparing these positions with the pseudo-three satellite case of Fig. 4.7, where SV-4 provides no horizontal position information, indicates that SV-1 and SV-2 assumed approximately the same

positions, while SV-3 moved to a position that provides more information along the semi-major axis to compensate for the loss of information from SV-4. In fact, SV-3 provides equal information in each axis direction of the emitter error ellipse.

The three satellite case in Fig. 4.9 indicates SV-3 is the primary satellite, while SV-1 and SV-2 have taken up positions providing information primarily along the semi-major axis, but also some information along the semi-minor axis. It is the tradeoff between this semi-major and semi-minor axis information that is instrumental in algorithm development. In the two satellite case, SV-2 is the primary satellite and SV-1 moves to the equal information position as shown in Fig. 4.10. These comparisons, then, form the basis for selection criteria.

Selection criteria are summarized as follows:

1. Primary satellite(s) should lie along the semi-major axis direction of the emitter error ellipse at an elevation of  $10-25^{\circ}$ .
2. Primary satellites should lie along the same LOS to reduce LOS bias errors.
3. Additional satellites should be selected to provide adequate information in the general semi-minor axis direction.

Satellites are selected which meet the criteria or come closest to satisfying them. Optimization results indicate that as the primary satellite(s) move closer to the semi-major axis direction, the additional satellite(s) move toward the equal information position. The three satellite case illustrates the situation where all the satellites are equally dominant, i.e. all are at approximately the same angle with respect to the semi-major axis of the emitter error ellipse. The selection algorithm must be implemented in such a way that, as less information is available along the semi-major axis direction, additional satellites are selected to provide information primarily along that direction.

The amount of change in emitter CEP as the satellites deviate from the optimum positions is addressed somewhat in this study, though not specifically. Gradient search data indicates that large changes in satellite azimuth can be made with relatively little effect on the CEP. This is encouraging because it opens a wider window for satellite selection, while maintaining a reasonable CEP. Data regarding CEP change versus satellite elevation is not so readily available, but changes in elevation in the range of interest (up to  $15^{\circ}$ ) should not result in significant increases in CEP.

## V. CONCLUSIONS AND RECOMMENDATIONS

### 5.1 CONCLUSIONS

This study shows that emitter location errors can be significantly reduced by selecting satellites according to the selection criteria presented in Chapter 4, rather than by minimum GDOP criteria. Three satellite performance is nearly as good as that obtained using four satellites, since only three satellites are necessary to determine the emitter horizontal position and user clock bias. When operation is further degraded to the two satellite case, emitter location is still slightly better than that obtained using four satellites selected to minimize GDOP.

Although the global minimum of the CEP cost function was not found, the local minima obtained for all of the fully determined cases agreed very closely. This indicates that little improvement in CEP can be expected beyond what is achieved in this study.

Iterating the error covariance matrix to steady-state after each satellite movement does not have a significant effect on either the final optimized satellite positions or on the minimum CEP obtained. This verifies the hypothesis by Lewantowicz (4) that using only a single iteration of the navigation Kalman

filter between satellite movements without reinitializing, does not significantly affect the results. Modifications to the gradient search routine did, however, result in more uniform, well-behaved "tracks" for the satellites as they moved to their optimum positions.

## 5.2 RECOMMENDATIONS

Since the weighted gradient search routine used in this study is highly unlikely to converge to the global minimum, another approach should be used that has a higher probability of finding the global minimum. It may be necessary to compute the cost at a very large number of random points in the eight-dimensional  $P_g$  space to identify candidate regions in which to perform gradient searches for the global minimum.

The computational loading required to perform the weighted gradient search to the local minimum is enormous. This is due in part to the nature of the gradient search, in that it tends to converge at a rapid rate initially, but converges very slowly as it nears the minimum. The possibility of searching initially using the weighted gradient method, since it guarantees that at least a local minimum will be found, and then switching to a more rapidly converging algorithm, such as the Newton-Raphson method, as the minimum cost is approached, should be explored.

The selection criteria established in Chapter 4 should be used to select satellites from a real-world constellation of available satellites. The emitter CEP obtained using these "optimum" satellites could then be compared to the CEP obtained using satellites selected using minimum GDOP criteria. This would provide a "real-world" performance evaluation of the emitter location system proposed in this study.

### Bibliography

1. Glazer, B.G. "GPS Receiver Operation," NAVIGATION, 25: 81-86 (Summer 1978).
2. Kane, Francis X. and John F. Scheerer. "The Global Role of NAVSTAR," Aerospace America, 42-46 (Jul 1984).
3. Kihara, Masahiko and Tsuyoshi Okada. "A Satellite Selection Method and Accuracy for the Global Positioning System," NAVIGATION, 31:8-20 (Spring 1984).
4. Lewantowicz, Zdzislaw H. Optimal Location of Uncooperative Emitters. MS thesis, CSDL-T-899. Massachusetts Institute of Technology, Cambridge, MA, December 1985.
5. Maher, Robert A. "A Comparison of Multichannel, Sequential, and Multiplex GPS Receivers for Air Navigation," NAVIGATION, 31: 96-111 (Summer 1984).
6. Maybeck, Peter S. Stochastic Models, Estimation, and Control, Volumes 1-3. New York: Academic Press, 1979.
7. Milliken, R.J. and C.J. Zoller. "Principles of Operation of NAVSTAR and System Characteristics," NAVIGATION, 25:3-14 (Summer 1978).
8. Spilker, J.J. "GPS Signal Structure and Performance Characteristics," NAVIGATION, 25: 29-54 (Summer 1978).
9. Sturza, Mark A. "GPS Navigation Using Three Satellites and a Precise Clock," NAVIGATION, 30: 146-156 (Summer 1983).
10. Torrieri, Don J. "Statistical Theory of Passive Location Systems," IEEE Transactions on Aerospace and Electronic Systems, AES-20: 183-198 (March 1984).

## Appendix A: Cost Gradient Function Derivation

The following appendix is taken in its entirety from the thesis by Lewantowicz (4:104-107).

## APPENDIX B

### COST GRADIENT FUNCTION DERIVATION

The cost function derived in Section 2.6 is

$$J = \text{tr} [EP^*] \quad (\text{B-1})$$

where  $E$  is an  $n \times n$  constant matrix consisting of zeros except for the two diagonal elements, corresponding to the two states that represent the horizontal emitter position errors, which are  $\sigma = 1.0$ . The matrix  $P^*$  is the  $n \times n$  symmetric error covariance matrix at time  $k$ . However, at a fixed  $k$ ,  $P^*$  is a function of only the variables with respect to which the cost  $J$  will be minimized.

The positions of GPS satellites or the positions of observers, or both, could be the variables of  $J$ . In fact, Chapter 4 covers optimization with respect to GPS positions, and Chapter 5 covers optimization with respect to both GPS and observer positions. Define the vector  $\underline{p}_g$  as the vector of those position variables. Then the cost  $J$  is a scalar function of  $\underline{p}_g$ .

$$\begin{aligned} J &= J \{P^*\} \\ &= J \{P^*[H]\} \\ &= J \{P^*[H(\underline{p}_g)]\} \end{aligned} \quad (\text{B-2})$$

where  $H$  is an  $m \times n$  measurement sensitivity matrix and  $\underline{p}_g$  is an  $i$  dimensioned vector.

In finding the minimum of a function, the cost gradient is used in several minimum cost search algorithms.

AD-A189 559

OPTIMAL SELECTION OF GLOBAL POSITIONING SYSTEM SET TO  
MINIMIZE EMITTER LO. (U) AIR FORCE INST OF TECH  
WRIGHT-PATTERSON AFB OH SCHOOL OF ENGI.. S G PETERS

2/2

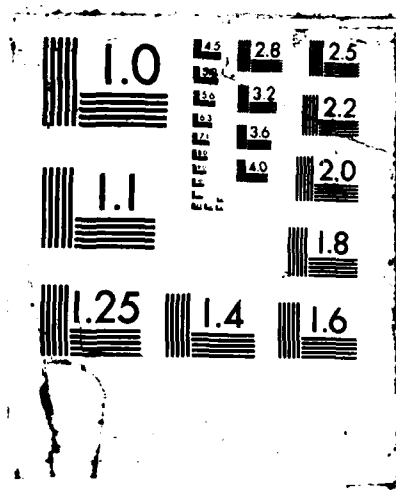
UNCLASSIFIED

DEC 87 AFIT/ENG/GE/87D-51

F/G 17/7

NL





$$\underline{g}^T = \frac{\partial J}{\partial \underline{P}_s} \quad (B-3)$$

Using the chain rule of partial derivatives

$$\underline{g}^T = \frac{\partial J}{\partial H} \frac{\partial H}{\partial \underline{P}_s} \quad (B-4)$$

where the first term is an  $m \times n$  matrix and the second term is  $m \times n \times 2$  third order tensor.

The first partial derivative term of Equation (B-4) is derived.

$$\begin{aligned} J &= \text{tr} [EP^+] \\ &= \text{tr} [E(H^T R^{-1} H + P^{-1})^{-1}] \end{aligned} \quad (B-5)$$

Then the variation in J is

$$\delta J = \text{tr} [E\delta P^+] \quad (B-6)$$

where  $\delta$  is the variation symbol

$$\begin{aligned} \delta P^+ &= - (H^T R^{-1} H + P^{-1})^{-1} (\delta H^T R^{-1} H + H^T R^{-1} \delta H) (H^T R^{-1} H + P^{-1})^{-1} \\ &= - P^+ (\delta H^T R^{-1} H + H^T R^{-1} \delta H) P^+ \end{aligned} \quad (B-7)$$

Therefore, Equation (B-6) becomes

$$\delta J = \text{tr} [-EP^+ (\delta H^T R^{-1} H + H^T R^{-1} \delta H) P^+] \quad (B-8)$$

however,

$$\text{tr} [AB] = \text{tr} [BA]$$

$$\delta J = \text{tr} [-P^+ EP^+ (\delta H^T R^{-1} H + H^T R^{-1} \delta H)] \quad (B-9)$$

however,  $\text{tr}[A] = \text{tr}[A^T]$

Thus the variation in cost J, with respect to the measurement sensitivity matrix H, becomes

$$\begin{aligned}\delta J &= \text{tr}[-P^+EP^+(H^TR^{-1}\delta H + H^TR^{-1}\delta H)] \\ &= -2 \text{tr}[P^+EP^+H^TR^{-1}\delta H]\end{aligned}\quad (B-10)$$

Using the result attributed to Kleinman, D.L. in [10]; given

$$f(X) = \text{tr}[M(X)] \quad (B-11)$$

where f is a scalar function of the matrix X, and M(X) is a matrix valued function of the matrix X then in

$$f(X + \epsilon \Delta X) - f(X) = \epsilon \text{tr}[M(X)\Delta X] \quad (B-12)$$

as  $\epsilon > 0$ . The derivative of a scalar function f with respect to the matrix valued variable X is

$$\frac{\partial f(X)}{\partial X} = M^T(X) \quad (B-13)$$

Thus the variation Equation (B-8), expressed as a partial derivative becomes

$$\begin{aligned}\frac{\partial J}{\partial H} &= -2[P^+EP^+H^TR^{-1}]^T \\ &= -2R^{-1}HP^+EP^+\end{aligned}\quad (B-14)$$

where  $\partial J/\partial H$  is an  $m \times n$  matrix.

Next, the  $\partial H / \partial \underline{P}_s$  is simply an element by element partial derivative of H with respect to each element of the vector  $\underline{P}_s$ . For  $\underline{P}_s$  of dimension l, there are l m x n matrices, the third-order tensor, of partial derivatives. Thus each component of the cost gradient vector is computed according to

$$\begin{aligned} \underline{g}^T &= \frac{\partial J}{\partial H} \frac{\partial H}{\partial \underline{P}_s} \\ &= \sum_{i=1}^m \sum_{j=1}^n \frac{\partial J}{\partial H}(i,j) \frac{\partial H}{\partial \underline{P}_s}(i,j) \end{aligned} \quad (B-15)$$

where  $\partial J / \partial H$  is computed as shown in (B-14). Computation of  $\partial H / \partial \underline{P}_s(k)$  matrices is presented in Appendices C and D for GPS only and for GPS with observer optimizations respectively.

## VITA

Captain Stephen G. Peters was born on 27 December 1954 in Croghan, New York. He graduated from Beaver River Central School in 1973 and attended the United States Air Force Academy from which he received the degree of Bachelor of Science in Engineering Sciences in June 1977. Upon graduation, he received a Regular commission in the USAF and was assigned to navigator and Electronic Warfare Officer training at Mather AFB, CA. Captain Peters then served tours flying the B-52 G/H at Grand Forks AFB, ND and the RC-135U at Offutt AFB, NE. He entered the Air Force Institute of Technology School of Engineering in May 1986. He is married to Wendy M.K. Peters and has two sons, Stanley and Sean.

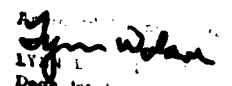
UNCLASSIFIED

SECURITY CLASSIFICATION OF THIS PAGE

0179 559

## REPORT DOCUMENTATION PAGE

Form Approved  
OMB No. 0704-0188

1a. REPORT SECURITY CLASSIFICATION UNCLASSIFIED			1b. RESTRICTIVE MARKINGS		
2a. SECURITY CLASSIFICATION AUTHORITY			3. DISTRIBUTION / AVAILABILITY OF REPORT Approved for public release; distribution unlimited.		
2b. DECLASSIFICATION / DOWNGRADING SCHEDULE					
4. PERFORMING ORGANIZATION REPORT NUMBER(S) AFIT/GE/ENG/87D-51			5. MONITORING ORGANIZATION REPORT NUMBER(S)		
6a. NAME OF PERFORMING ORGANIZATION School of Engineering		6b. OFFICE SYMBOL (If applicable) AFIT/ENG		7a. NAME OF MONITORING ORGANIZATION	
6c. ADDRESS (City, State, and ZIP Code) Air Force Institute of Technology Wright-Patterson AFB, OH 45433-6853				7b. ADDRESS (City, State, and ZIP Code)	
8a. NAME OF FUNDING / SPONSORING ORGANIZATION		8b. OFFICE SYMBOL (If applicable)		9. PROCUREMENT INSTRUMENT IDENTIFICATION NUMBER	
8c. ADDRESS (City, State, and ZIP Code)				10. SOURCE OF FUNDING NUMBERS	
		PROGRAM ELEMENT NO.		PROJECT NO.	TASK NO.
				WORK UNIT ACCESSION NO.	
11. TITLE (Include Security Classification) See Box 19					
12. PERSONAL AUTHOR(S) Stephen G. Peters, B.S., Capt. USAF					
13a. TYPE OF REPORT MS Thesis		13b. TIME COVERED FROM _____ TO _____		14. DATE OF REPORT (Year, Month, Day) 1987 December	
				15. PAGE COUNT 97	
16. SUPPLEMENTARY NOTATION					
17. COSATI CODES			18. SUBJECT TERMS (Continue on reverse if necessary and identify by block number)		
FIELD	GROUP	SUB-GROUP			
17	11		Global Positioning System, Position Finding, Direction Finding		
19. ABSTRACT (Continue on reverse if necessary and identify by block number)					
Title: OPTIMAL SELECTION OF GLOBAL POSITIONING SYSTEM SET TO MINIMIZE EMITTER LOCATION ERRORS					
Thesis Chairman: Zdzislaw H. Lewantowicz, Lt Col, USAF Deputy Department Head, Department of Electrical and Computer Engineering					
 21 Apr 87 Deputy for Research and Professional Development Air Force Institute of Technology (AFIT) Wright-Patterson AFB OH 45433					
20. DISTRIBUTION / AVAILABILITY OF ABSTRACT <input checked="" type="checkbox"/> UNCLASSIFIED/UNLIMITED <input type="checkbox"/> SAME AS RPT <input type="checkbox"/> DTIC USERS			21. ABSTRACT SECURITY CLASSIFICATION UNCLASSIFIED		
22a. NAME OF RESPONSIBLE INDIVIDUAL Zdzislaw H. Lewantowicz, Lt Col, USAF			22b. TELEPHONE (Include Area Code) (513) 255-3576		22c. OFFICE SYMBOL AFIT/ENG

UNCLASSIFIED

4  
The use of the Global Positioning System (GPS) as a navigation aid for aircraft attempting to locate a ground based electromagnetic energy emitter is studied. In particular, the satellite geometry which yields minimum errors in the emitter location estimation for four different satellite availability cases is explored. This geometry, in general, is not the same as that which yields minimum aircraft navigation errors. Satellite selection criteria are identified and serve as a basis for selection algorithm development.

The research shows that emitter location errors can be significantly reduced by selecting satellites based on the criteria presented in this study. Three satellite performance is found to be nearly as good as that obtained using four satellites and, for the two satellite case, emitter location is still better for some period of time than that obtained using four satellites selected to minimize Geometric Dilution of Precision (GDOP).

X  
/

UNCLASSIFIED

END

DATE

FILMED

MARCH

1988

DTIC